Title	Chiral behavior of $K \to \pi l \nu$ decay form factors in lattice QCD with exact chiral symmetry
Author(s)	Aoki, S.; Cossu, G.; Feng, X.; Fukaya, H.; Hashimoto, S.; Kaneko, T.; Noaki, J.; Onogi, T.; JLQCD Collaboration
Citation	Physical Review D (2017), 96(3)
Issue Date	2017-08-01
URL	http://hdl.handle.net/2433/250295
Right	© 2017 American Physical Society
Type	Journal Article
Textversion	publisher

Chiral behavior of $K \to \pi l \nu$ decay form factors in lattice QCD with exact chiral symmetry

S. Aoki,[1] G. Cossu,[2] X. Feng,[3,4] H. Fukaya,[5] S. Hashimoto,[6,7] T. Kaneko,[6,7] J. Noaki,[6] and T. Onogi[5]
(JLQCD Collaboration)

[1]*Yukawa Institute for Theoretical Physics, Kyoto University, Kyoto 606-8502, Japan*
[2]*School of Physics and Astronomy, The University of Edinburgh, Edinburgh EH9 3JZ, United Kingdom*
[3]*Physics Department, Columbia University, New York, New York 10027, USA*
[4]*School of Physics, Peking University, Beijing 100871, China*
[5]*Department of Physics, Osaka University, Osaka 560-0043, Japan*
[6]*High Energy Accelerator Research Organization (KEK), Ibaraki 305-0801, Japan*
[7]*School of High Energy Accelerator Science, SOKENDAI (The Graduate University for Advanced Studies), Ibaraki 305-0801, Japan*

(Received 8 May 2017; published 3 August 2017)

We calculate the form factors of the $K \to \pi l \nu$ semileptonic decays in three-flavor lattice QCD and study their chiral behavior as a function of the momentum transfer and the Nambu-Goldstone boson masses. Chiral symmetry is exactly preserved by using the overlap quark action, which enables us to directly compare the lattice data with chiral perturbation theory (ChPT). We generate gauge ensembles at a lattice spacing of 0.11 fm with four pion masses covering 290–540 MeV and a strange quark mass m_s close to its physical value. By using the all-to-all quark propagator, we calculate the vector and scalar form factors with high precision. Their dependence on m_s and the momentum transfer is studied by using the reweighting technique and the twisted boundary conditions for the quark fields. We compare the results for the semileptonic form factors with ChPT at next-to-next-to-leading order in detail. While many low-energy constants appear at this order, we make use of our data of the light meson electromagnetic form factors in order to control the chiral extrapolation. We determine the normalization of the form factors as $f_+(0) = 0.9636(36)(^{+57}_{-35})$ and observe reasonable agreement of their shape with experiment.

DOI: 10.1103/PhysRevD.96.034501

I. INTRODUCTION

The kaon semileptonic decays $K \to \pi l \nu$ provide a precise determination of the Cabibbo-Kobayashi-Maskawa (CKM) matrix element $|V_{us}|$. The decay rate is given as

$$\Gamma(K \to \pi l \nu) = \frac{G_F^2 M_K^5}{192\pi^3} C^2 S_{\mathrm{EW}} (1 + \delta_{\mathrm{EM}} + \delta_{SU(2)})^2 I |V_{us}|^2 f_+(0)^2, \tag{1}$$

where G_F is the Fermi constant, the Clebsch-Gordan coefficient C is 1 $(1/\sqrt{2})$ for the K^0 $(K^\pm)$ decay, and I represents the phase space integral. We denote the short-distance electroweak, long-distance electromagnetic (EM), and isospin-breaking corrections by S_{EW}, δ_{EM} and $\delta_{SU(2)}$, respectively.

The vector form factor $f_+(t)$ is defined from the relevant hadronic matrix element,

$$\langle \pi(p') | V_\mu | K(p) \rangle = (p + p')_\mu f_+(t) + (p - p')_\mu f_-(t), \tag{2}$$

where $t = (p' - p)^2$ is the momentum transfer. Instead of $f_-(t)$, the scalar form factor,

$$f_0(t) = f_+(t) + \frac{t}{M_K^2 - M_\pi^2} f_-(t), \tag{3}$$

has been widely used in phenomenological analyses of the semileptonic decays. By definition, the normalizations of the vector and scalar form factors coincide with each other at the zero momentum transfer $t = 0$,

$$f_+(0) = f_0(0). \tag{4}$$

The Ademollo-Gatto theorem [1,2] states that SU(3) breaking effects are suppressed as $f_+(0) = 1 + O((m_l - m_s)^2)$, where $m_l = (m_u + m_d)/2$ and $m_{\{u,d,s\}}$ represent the masses of up, down and strange quarks. The normalization $f_+(0)$ has been used, therefore, as an important input to determine $|V_{us}|$ through the decay rate (1).

Since the form factors describe effects due to the strong interaction at low energy, a precise calculation of $f_+(0)$ needs a nonperturbative method to study QCD. A target accuracy is $\lesssim 1\%$, because other experimental and

theoretical inputs have been determined with a similar or even better accuracy [3,4]. Lattice QCD is the only known method to calculate the form factors with controlled and systematically improvable accuracy.

The phase space integral I encodes information about the shape of the form factors, namely their t dependence. The current determination of $|V_{us}|$ employs a precise estimate of I obtained from experimental data. A lattice study of the form factor shape and comparison with experiments can examine the reliability of the numerical lattice determination of the normalization $f_+(0)$. We note that new physics can modify not only the normalization but also the shape, which may, therefore, provide a different probe of new physics if both theoretical and experimental data become sufficiently accurate in the future.

Lattice calculation of $f_+(0)$ has become mature [4–6] by realistic simulations at reasonably small pion masses and lattice spacings. The so-called twisted boundary condition [7] enables us to simulate near the reference point $t \simeq 0$. Although recent lattice studies [8–11] have achieved subpercent accuracy, more independent calculations are welcome to establish the lattice estimate with such a high precision. A detailed study of the form factor shape based on the next-to-leading order (NLO) chiral perturbation theory (ChPT) [12–14] and model independent parametrization [15–17] is also available [11].

A recent trend of precision calculations is to directly simulate physical quark masses at $t = 0$. In this study, we take a different approach based on our large-scale simulations with exact chiral symmetry [18]. By exploiting exact symmetry, we directly compare our lattice data with next-to-next-to-leading order (NNLO) ChPT [19,20], and determine the normalization $f_+(0)$, relevant low-energy constants (LECs) in the ChPT Lagrangian, and study the form factor shape. We note that chiral symmetry is explicitly violated with conventional lattice actions. The explicit violation makes the direct comparison between lattice QCD and NNLO ChPT difficult because of modified functional form of the ChPT formulas and additional unknown LECs.

For a rigorous comparison with ChPT, we calculate the form factors with high precision by using the so-called all-to-all quark propagator [21,22]. The strange quark mass dependence and the form factor shape near the reference point $t = 0$ are studied by employing the reweighting technique [23,24] and the twisted boundary conditions, respectively. While many unknown LECs appear at NNLO, we control the chiral extrapolation by making use of our lattice data of the light meson EM form factors obtained in Ref. [25]. We also employ a linear combination of f_0 and the decay constant ratio F_K/F_π [20], which has a reduced number of the LECs. Our preliminary analyses have been reported in Refs. [26–29].

This paper is organized as follows. In Sec. II, we introduce our method to generate our gauge ensembles and to calculate relevant meson correlators. The kaon semileptonic form factors are extracted at our simulation points in Sec. III. Section IV details comparison with NNLO ChPT to study the chiral behavior of the form factors, and summarizes the numerical results for the normalization, shape and relevant LECs. We summarize our conclusions in Sec. V.

II. SIMULATION METHOD

A. Configuration generation

We simulate $N_f = 2 + 1$ QCD using the overlap quark action [30,31] defined by the Dirac operator,

$$D(m_q) = \left(1 - \frac{m_q}{2m_0}\right) D(0) + m_q, \tag{5}$$

where m_q represents the quark mass, and

$$D(0) = m_0(1 + \gamma_5 \mathrm{sgn}[H_{\mathrm{W}}(-m_0)]) \tag{6}$$

is the overlap-Dirac operator in the massless limit. The parameter m_0 for the Hermitian Wilson-Dirac operator H_W is set to $m_0 = 1.6$ from our study of the locality of D [32]. Numerical simulations are remarkably accelerated by modifying the Iwasaki gauge action [33] with an auxiliary Boltzmann weight [34,35]

$$\Delta_{\mathrm{W}} = \frac{\det[H_{\mathrm{W}}(-m_0)^2]}{\det[H_{\mathrm{W}}(-m_0)^2 + \mu^2]} \quad (\mu = 0.2) \tag{7}$$

and by simulating the trivial topological sector. The effect of the fixed *global* topology can be considered as a finite volume effect suppressed by the inverse lattice volume [36]. In fact, the effect turns out to be small in our previous study of the pion EM form factor on similar and even smaller lattice volumes [25,37]. We also note that local topological excitations are active in our gauge ensembles. Indeed, the topological susceptibility calculated in our simulations is nicely consistent with the prediction of ChPT [38].

The lattice spacing a determined from the Ω baryon mass is 0.112(1) fm with our choice of the gauge coupling $\beta = 6/g^2 = 2.30$. We simulate four values of the degenerate up and down quark masses m_l. The bare masses are 0.015, 0.025, 0.035 and 0.050 in lattice units, and cover a range of $M_\pi \sim 290$–540 MeV. The gauge ensembles are generated at a strange quark mass $m_s = 0.080$, close to its physical value $m_{s,\mathrm{phys}} = 0.081$. The m_s dependence of the form factors is studied by calculating them at a different $m_s(= 0.060)$ using the reweighting technique [23,24].

The spatial lattice size is set to $N_s = L/a = 24$ or 16 depending on m_l, so that a condition $M_\pi L \gtrsim 4$ is satisfied to control finite volume effects. The temporal lattice size is fixed to $N_t = T/a = 48$. The statistics are 2,500 HMC

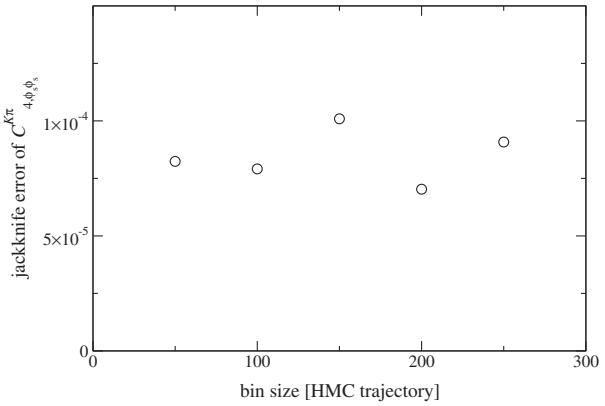

FIG. 1. Jackknife error of three-point function $C^{K\pi}_{4,\phi_s,\phi_s}(\Delta x_4, \Delta x_4', \mathbf{p}, \mathbf{p}')$ as a function of bin size. We plot data at $(m_{ud}, m_s) = (0.015, 0.080)$ with $\Delta x_4 = \Delta x_4' = 9$, $\theta = 0.00$, and $\theta' = 1.68$. See Sec. II B for the definition and parameters of the three-point function.

trajectories at each simulation point (m_l, m_s). We estimate the statistical error by the jackknife method with a bin size of 50 trajectories. Figure 1 shows that the jackknife error of three-point functions is stable against the choice of the bin size. Our simulation parameters are summarized in Table I.

B. Calculation of meson correlators

We calculate the three-point functions of the kaon and pion,

$$C^{PQ}_{\mu,\phi\phi'}(\Delta x_4, \Delta x_4'; \mathbf{p}, \mathbf{p}') = \frac{1}{N_t}\sum_{x_4=1}^{N_t}\sum_{\mathbf{x},\mathbf{x}',\mathbf{x}''}\langle \mathcal{O}_{Q,\phi'}(\mathbf{x}'', x_4 + \Delta x_4 + \Delta x_4'; \mathbf{p}') \times V_\mu(\mathbf{x}', x_4 + \Delta x_4)\mathcal{O}_{P,\phi}(\mathbf{x}, x_4; \mathbf{p})^\dagger\rangle, \quad (8)$$

where P (Q) specifies the initial (final) meson, and is "K" or "π." The vector current V_μ is the weak current for $P \neq Q$, and light $(\bar{l}\gamma_\mu l)$ or strange current $(\bar{s}\gamma_\mu s)$ for $P = Q$. The initial (final) meson momentum is denoted by $\mathbf{p}^{(\prime)}$, whereas $\Delta x_4{}^{(\prime)}$ is the temporal separation between V_μ and the meson source (sink) operator $\mathcal{O}^\dagger_{P,\phi}$ ($\mathcal{O}_{Q,\phi'}$). We also calculate the two-point function,

$$C^{P}_{\phi\phi'}(\Delta x_4; \mathbf{p}) = \frac{1}{N_t}\sum_{x_4=1}^{N_t}\sum_{\mathbf{x}',\mathbf{x}}\langle \mathcal{O}_{P,\phi'}(\mathbf{x}', x_4 + \Delta x_4; \mathbf{p}) \times \mathcal{O}_{P,\phi}(\mathbf{x}, x_4; \mathbf{p})^\dagger\rangle, \quad (9)$$

to extract the form factors below the maximum value of the momentum transfer $t_{\max} = (M_K - M_\pi)^2$ (see Sec. III for details).

The meson interpolating field is given as

$$\mathcal{O}_{P,\phi}(\mathbf{x}, x_4, \mathbf{p}) = \sum_{\mathbf{r}}\phi(\mathbf{r})\bar{q}'(\mathbf{x} + \mathbf{r}, x_4)\gamma_5 q(\mathbf{x}, x_4). \quad (10)$$

In addition to the simple local operator with $\phi_l(\mathbf{r}) = \delta_{\mathbf{r},\mathbf{0}}$, we also use an exponentially smeared operator with $\phi_s(\mathbf{r}) = \exp[-0.4|\mathbf{r}|]$ to reduce the excited state contamination in the meson correlation functions.

There are no explicit Fourier factors in the above expressions (8) and (9). The meson momentum $\mathbf{p}^{(\prime)}$ is induced through the twisted boundary condition for the valence quark fields [7]

$$q(\mathbf{x} + L\hat{k}, x_4) = e^{i\theta}q(\mathbf{x}, x_4),$$
$$\bar{q}(\mathbf{x} + L\hat{k}, x_4) = e^{-i\theta}\bar{q}(\mathbf{x}, x_4) \quad (k = 1, 2, 3). \quad (11)$$

Here $\hat{k}$ is a unit vector in the k-th direction, and we take a common twist angle θ in all three spatial directions for simplicity. This condition induces a quark momentum of $p_k = \theta/L \leq 2\pi/L$, and hence a meson momentum $p_k = (\theta - \theta')/L$ by using different twist angles, θ and θ', for the quark and anti-quark components. With our choices of the twist angle listed in Table I, we simulate a region of the momentum transfer $-(300\ \text{MeV})^2 \lesssim t \leq t_{\max}$. The important reference point $t = 0$ is located inside this region. Our studies of the EM form factors of charged pion and kaon [25,37] suggest that the next-to-next-to-next-to-leading order (N^{3}LO) chiral correction, which is not known in ChPT, is small in this region of t.

In Eqs. (8) and (9), the summation over the source location $(\mathbf{x}, x_4)$ is not mandatory, but is helpful to remarkably improve the statistical accuracy. To this end, we need the so-called all-to-all quark propagator, which flows from any lattice site to any site. Since a naive calculation is prohibitively time consuming, we construct the all-to-all propagator by using low-lying modes of the overlap-Dirac operator [21,22] and the stochastic noise method [39]. Namely, the low-mode contribution is calculated as

TABLE I. Simulation parameters. Meson masses, M_π and M_K, are in units of MeV.

lattice	m_l	m_s	M_π	M_K	θ
$16^3 \times 48$	0.050	0.080	540(3)	617(4)	0.00, 0.40, 0.96, 1.60
$16^3 \times 48$	0.035	0.080	453(4)	578(4)	0.00, 0.60, 1.28, 1.76
$24^3 \times 48$	0.025	0.080	379(2)	548(3)	0.00, 1.68, 2.64
$24^3 \times 48$	0.015	0.080	293(2)	518(1)	0.00, 1.68, 2.64
$16^3 \times 48$	0.050	0.060	540(4)	567(4)	0.00, 0.40, 0.96, 1.60
$16^3 \times 48$	0.035	0.060	451(6)	524(5)	0.00, 0.60, 1.28, 1.76
$24^3 \times 48$	0.025	0.060	378(7)	492(7)	0.00, 1.68, 2.64
$24^3 \times 48$	0.015	0.060	292(3)	459(4)	0.00, 1.68, 2.64

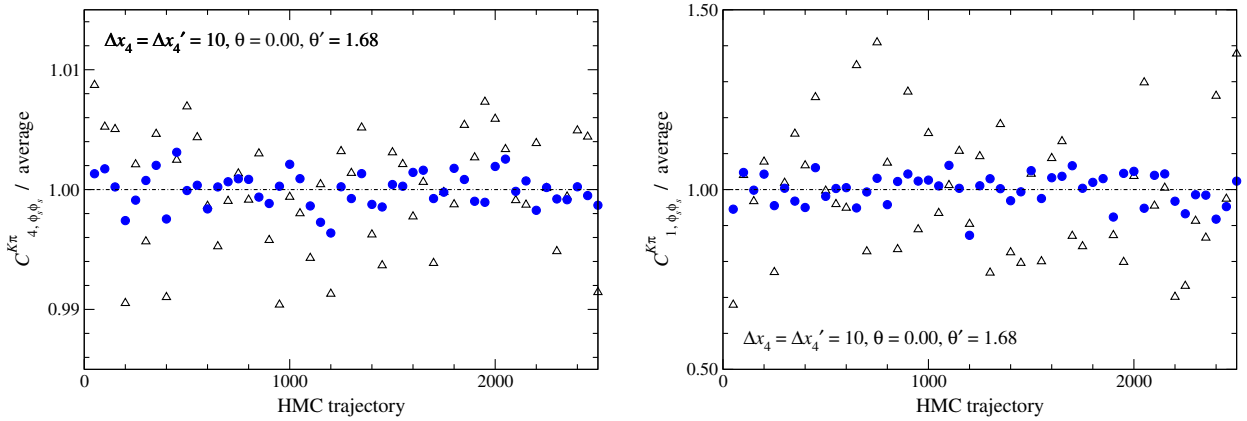

FIG. 2. Statistical fluctuation of three-point function $C^{K\pi}_{\mu,\phi_s\phi_s}(\Delta x_4, \Delta x_4'; \mathbf{p}, \mathbf{p}')$ for $\mu = 4$ (left panel) and 1 (right panel). We plot the value for each jackknife sample normalized by the statistical average. The horizontal axis represents the HMC trajectory count of the excluded configuration in the jackknife analysis. The data are obtained at $(m_l, m_s) = (0.015, 0.080)$ with $\Delta x_4 = \Delta x_4' = 10$, $\theta = 0.00$, $\theta' = 1.68$. Triangles and circles are data before and after averaging over the temporal location of the source operator x_4, respectively.

$$\{D(m_q)^{-1}\}_{\text{low}}(x,y) = \sum_{k=1}^{N_e} \frac{1}{\lambda_k^{(q)}} u_k(x) u_k^\dagger(y), \quad (12)$$

where $\lambda_k^{(q)}$ and u_k represent the k-th lowest eigenvalue of $D(m_q)$ and its associated eigenvector. The number of the low-modes is $N_e = 240$ and 160 on the $24^3 \times 48$ and $16^3 \times 48$ lattices, respectively.

We estimate the remaining contribution from higher modes stochastically by using the noise method together with the dilution technique [22]. A complex Z_2 noise vector is prepared for each configuration, and is split into $N_d = 3 \times 4 \times N_t/2$ vectors $\eta_d(x)(d = 1, \ldots, N_d)$. These diluted noise vectors have nonzero elements only for a single combination of color and spinor indices and at two consecutive time slices. We solve a linear equation for each diluted noise vector

$$D(m_q) x_q = P_{\text{high}} \eta_d \quad (d = 1, \ldots, N_d), \quad (13)$$

where $P_{\text{high}} = 1 - P_{\text{low}}$, and $P_{\text{low}} = \sum_{k=1}^{N_e} u_k u_k^\dagger$ is the projector to the eigenspace spanned by the low-modes. The high-mode contribution is then estimated as

$$\{D(m_q)^{-1}\}_{\text{high}}(x,y) = \sum_{d=1}^{N_d} x_d^{(q)}(x) \eta_d^\dagger(y). \quad (14)$$

We refer the readers to Refs. [25,37] for more details on our implementation.

Figure 2 shows the statistical fluctuation of the three-point function $C^{K\pi}_{\mu,\phi_s\phi_s}(\Delta x_4, \Delta x_4'; \mathbf{p}, \mathbf{p}')$ with a certain choice of $\Delta x_4{}^{(\prime)}$ and $\mathbf{p}^{(\prime)}$. Averaging over the temporal coordinate x_4 reduces the statistical error by about a factor of 3 for the temporal component $\mu = 4$ and a factor of 5 for spatial $\mu = 1$.

The m_s dependence of the form factors is studied by repeating our calculation at a different value of the strange quark mass $m_s' = 0.060$ using the gauge ensemble at $m_s = 0.040$ and the reweighing technique [23,24]. For instance, the three-point function can be calculated as

$$\langle C^{PQ}_{\mu,\phi\phi'} \rangle_{m_s'} = \langle C^{PQ}_{\mu,\phi\phi'} \tilde{w}(m_s', m_s) \rangle_{m_s}, \quad (15)$$

where $\langle \cdots \rangle_{m_s^{(\prime)}}$ represents the Monte Carlo average at $m_s^{(\prime)}$. The reweighting factor $\tilde{w}$ from m_s to m_s' is defined as

$$\tilde{w}(m_s', m_s) = \frac{w(m_s', m_s)}{\langle w(m_s', m_s) \rangle_{m_s}}, \quad w(m_s', m_s) = \det\left[\frac{D(m_s')}{D(m_s)}\right] \quad (16)$$

for each gauge configuration. In order to remarkably reduce the computational cost, w is decomposed into contributions from low and high modes

$$w(m_s', m_s) = w_{\text{low}}(m_s', m_s) w_{\text{high}}(m_s', m_s), \quad (17)$$

$$w_{\text{low(high)}}(m_s', m_s) = \det\left[P_{\text{low(high)}} \frac{D(m_s')}{D(m_s)} P_{\text{low(high)}}\right]. \quad (18)$$

We exactly calculate the low mode contribution w_{low} by using the low-lying eigenvalues, whereas the high-mode contribution w_{high} is estimated through a stochastic estimator for its square

$$w^2_{\text{high}}(m_s', m_s) = \frac{1}{N_r} \sum_{r=1}^{N_r} e^{-\frac{1}{2}(P_{\text{high}}\xi_r)^\dagger (\Omega - 1) P_{\text{high}} \xi_r}, \quad (19)$$

where $\Omega \equiv D(m_s)^\dagger \{D(m_s')^{-1}\}^\dagger D(m_s')^{-1} D(m_s)$. In our study of the EM form factors [25], the full reweighting

factor ω turned out to be largely dominated by the low-mode contribution $w_{\rm low}$ with our simulation setup. For each configuration, therefore, we use only ten Gaussian random vectors $\{\xi_1, \ldots, \xi_{10}\}$ ($N_r = 10$) with which the uncertainty of $\tilde{w}$ due to the stochastic estimator is negligibly small compared to its statistical fluctuation.

III. FORM FACTORS AT SIMULATION POINTS

In the limit of large temporal separations $\Delta x_4, \Delta x_4' \to \infty$, the light meson three-point function (P, $Q = \pi$ or K) is dominated by the ground state contribution as

$$C^{PQ}_{\mu,\phi\phi'}(\Delta x_4, \Delta x_4'; \mathbf{p}, \mathbf{p}') \xrightarrow[\Delta x_4, \Delta x_4' \to \infty]{} \frac{Z_{Q,\phi'}(\mathbf{p}')^* Z_{P,\phi}(\mathbf{p})}{4E_Q(\mathbf{p}')E_P(\mathbf{p})} \frac{1}{Z_V} \langle Q(p')|V_\mu|P(p)\rangle \times e^{-E_Q(\mathbf{p}')\Delta x_4'} e^{-E_P(\mathbf{p})\Delta x_4}, \tag{20}$$

where $Z_{P,\phi}(\mathbf{p}) = \langle P(p)|\mathcal{O}_{P,\phi}\rangle$ is the overlap of the meson interpolating field to the physical state, and Z_V is the renormalization factor for the vector current. These factors and the exponential damping factors $e^{-E_{P(Q)}(\mathbf{p}^{(\prime)})\Delta x_4^{(\prime)}}$ cancel in the following double ratio [40,41]

$$R_{\phi\phi'}(\Delta x_4, \Delta x_4') = \frac{C^{K\pi}_{4,\phi\phi'}(\Delta x_4, \Delta x_4'; \mathbf{0}, \mathbf{0}) C^{\pi K}_{4,\phi\phi'}(\Delta x_4, \Delta x_4'; \mathbf{0}, \mathbf{0})}{C^{KK}_{4,\phi\phi'}(\Delta x_4, \Delta x_4'; \mathbf{0}, \mathbf{0}) C^{\pi\pi}_{4,\phi\phi'}(\Delta x_4, \Delta x_4'; \mathbf{0}, \mathbf{0})} \xrightarrow[\Delta x_4, \Delta x_4' \to \infty]{} \frac{(M_K + M_\pi)^2}{4M_K M_\pi} f_0(t_{\rm max})^2, \tag{21}$$

from which we calculate the scalar form factor $f_0(t_{\rm max})$ at the largest momentum transfer $t_{\rm max}$. Figure 3 shows the effective value of $f_0(t_{\rm max})$ as a function of Δx_4. The accuracy of $f_0(t_{\rm max})$ is typically $\lesssim 1\%$ with our simulation setup. The figure also demonstrates that the all-to-all quark propagator greatly helps us increase the reliability of the precision calculation of $f_0(t_{\rm max})$: it enables us to confirm the consistency in $f_0(t_{\rm max})$ among different values of $\Delta x_4 + \Delta x_4'$ and different smearing functions for the meson interpolating fields.

At smaller momentum transfer $t < t_{\rm max}$, the vector form factor $f_+(t)$ and the ratio $\xi(t) = f_-(t)/f_+(t)$ are calculated from the following ratios [41–43]

$$\tilde{R}_{\phi\phi'}(\mathbf{p}, \mathbf{p}'; \Delta x_4, \Delta x_4') = \frac{C^{K\pi}_{4,\phi\phi'}(\Delta x_4, \Delta x_4'; \mathbf{p}, \mathbf{p}') C^{K}_{\phi\phi_l}(\Delta x_4, \mathbf{0}) C^{\pi}_{\phi_l\phi'}(\Delta x_4', \mathbf{0})}{C^{K\pi}_{4,\phi\phi'}(\Delta x_4, \Delta x_4'; \mathbf{0}, \mathbf{0}) C^{K}_{\phi\phi_l}(\Delta x_4, \mathbf{p}) C^{\pi}_{\phi_l\phi'}(\Delta x_4', \mathbf{p}')} \xrightarrow[\Delta x_4, \Delta x_4' \to \infty]{} \left\{ \frac{E_K(\mathbf{p}) + E_\pi(\mathbf{p}')}{M_K + M_\pi} + \frac{E_K(\mathbf{p}) - E_\pi(\mathbf{p}')}{M_K + M_\pi} \xi(t) \right\} \frac{f_+(t)}{f_0(t_{\rm max})}, \tag{22}$$

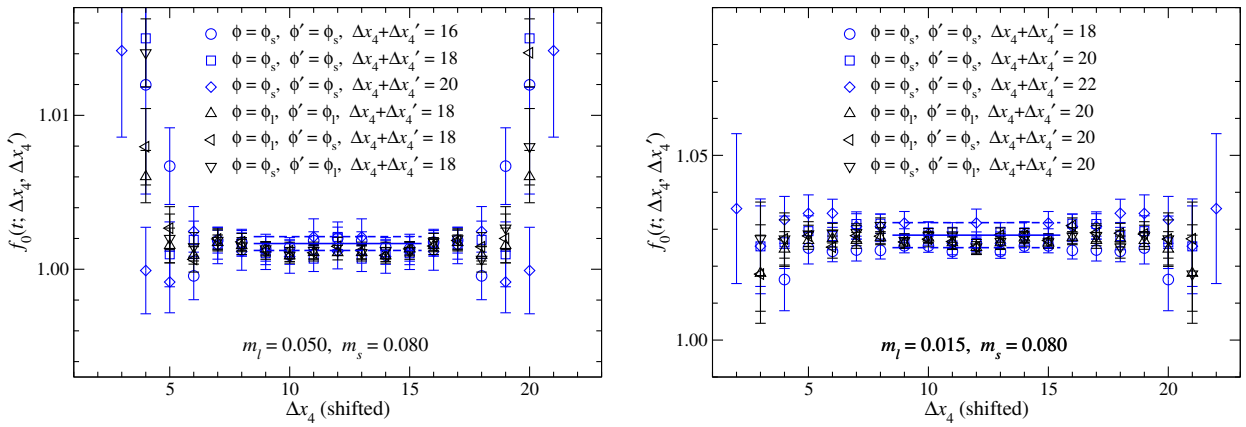

FIG. 3. Effective value of $f_0(t_{\rm max})$ estimated from double ratio $R_{\phi\phi'}(\Delta x_4, \Delta x_4')$ at $(m_l, m_s) = (0.050, 0.080)$ (left panel) and (0.015,0.080) (right panel). Blue circles, squares and diamond show data with the smeared source and sink for different values of $\Delta x_4 + \Delta x_4'$. On the other hand, black triangles show data with local source and/or sink with $\Delta x_4 + \Delta x_4'$ kept fixed. All data are shifted along the horizontal axis so that the meson source and sink operators are located at $T/4 - (\Delta x_4 + \Delta x_4')/2$ and $T/4 + (\Delta x_4 + \Delta x_4')/2$, respectively. Solid and dashed lines show a constant fit to data with different values of Δx_4 and $\Delta x_4 + \Delta x_4'$.

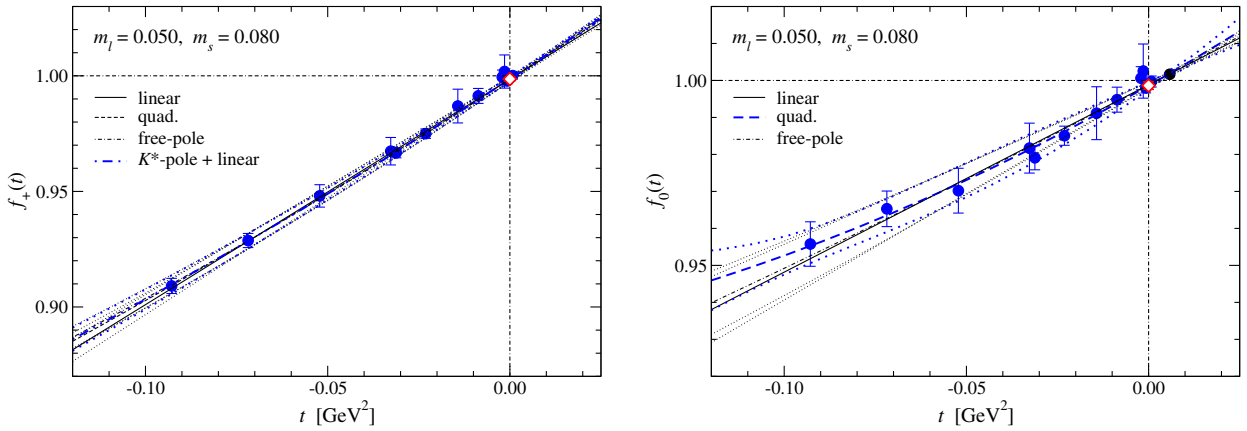

FIG. 4. Vector (left panel) and scalar form factors (right panel) as a function of t at $(m_l, m_s) = (0.050, 0.080)$. Solid circles show the results at simulated t's. Solid, dashed and dot-dashed lines are linear, quadratic (26) and free-pole fits (27), respectively. We also plot the fit with the K^* pole (25) for f_+. The dotted lines show their statistical error. The value interpolated to $t = 0$ is shown by the open diamond. The blue thicker lines show the fit to estimate the central value and statistical error of the interpolated value.

$$R_{k,\phi\phi'}(\mathbf{p},\mathbf{p}';\Delta x_4,\Delta x_4') = \frac{C^{K\pi}_{k,\phi\phi'}(\Delta x_4,\Delta x_4';\mathbf{p},\mathbf{p}')C^{KK}_{4,\phi\phi'}(\Delta x_4,\Delta x_4';\mathbf{p},\mathbf{p}')}{C^{K\pi}_{4,\phi\phi'}(\Delta x_4,\Delta x_4';\mathbf{p},\mathbf{p}')C^{KK}_{k,\phi\phi'}(\Delta x_4,\Delta x_4';\mathbf{p},\mathbf{p}')} \xrightarrow[\Delta x_4,\Delta x_4'\to\infty]{} \frac{E_K(\mathbf{p})+E_K(\mathbf{p}')}{(p+p')_k}\frac{(p+p')_k+(p-p')_k\xi(t)}{E_K(\mathbf{p})+E_\pi(\mathbf{p}')+\{E_K(\mathbf{p})-E_\pi(\mathbf{p}')\}\xi(t)}. \tag{23}$$

The last line of Eq. (22) assumes the asymptotic form of the two-point function

$$C^P_{\phi\phi'}(\Delta x_4;\mathbf{p}) \xrightarrow[\Delta x_4\to\infty]{} \frac{Z_{P,\phi'}(\mathbf{p})^* Z_{P,\phi}(\mathbf{p})}{2E_P(\mathbf{p})} e^{-E_P(\mathbf{p})\Delta x_4}. \tag{24}$$

We evaluate $f_0(t)$ from $f_+(t)$ and $\xi(t)$ at $t < t_{\rm max}$. Note that, at $t_{\rm max}$, we only have results for $f_0(t_{\rm max})$ from $R_{\phi\phi'}$, since $\tilde{R}_{\phi\phi'}$ and $R_{k,\phi\phi'}$ have no sensitivity to f_+ and ξ.

In Figs. 4 and 5, we plot the vector and scalar form factors as a function of t. At $m_s = 0.080$, the statistical accuracy of the nontrivial chiral correction $f_{\{+,0\}}(t) - 1$ due to $m_s \neq m_l$ and $t \neq 0$ is typically 10%–20%. Analyses based on ChPT suggest that finite volume effects including those due to the twisted boundary condition [44] are below this accuracy: $O(\exp[-M_\pi L]) \lesssim O(2\%)$ or less [44–46].

In Fig. 6, we observe that the statistical error is about a factor of two larger at $m_s = 0.060$ due to reweighting.

We parametrize the t dependence of the form factors $f_{\{+,0\}}$ to estimate the normalization $f_+(0) = f_0(0)$ and the slopes $df_{\{+,0\}}/dt|_{t=0}$ at simulated quark masses. For the vector form factor f_+, we use the following parametrization based on the vector meson dominance (VMD) hypothesis

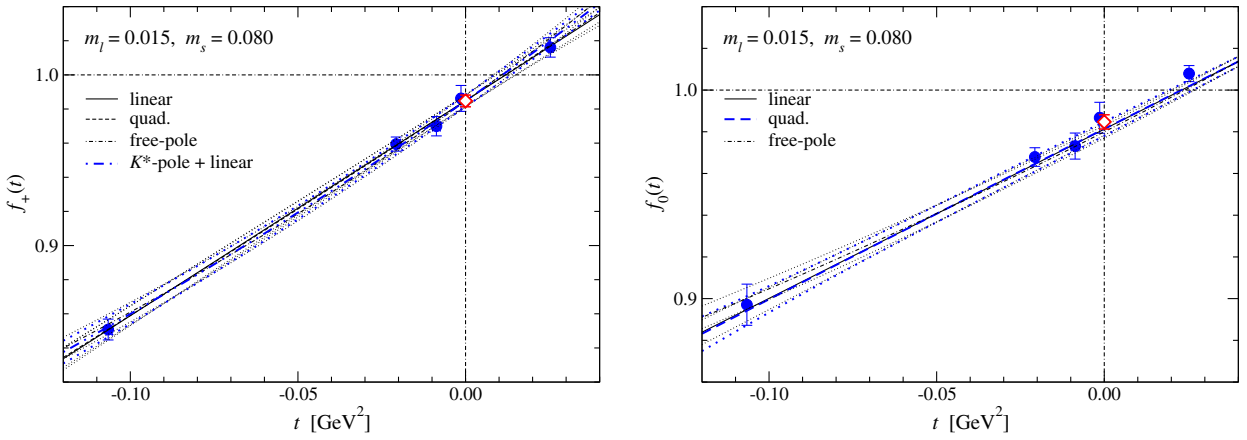

FIG. 5. Same as Fig. 4, but for $(m_l, m_s) = (0.015, 0.080)$.

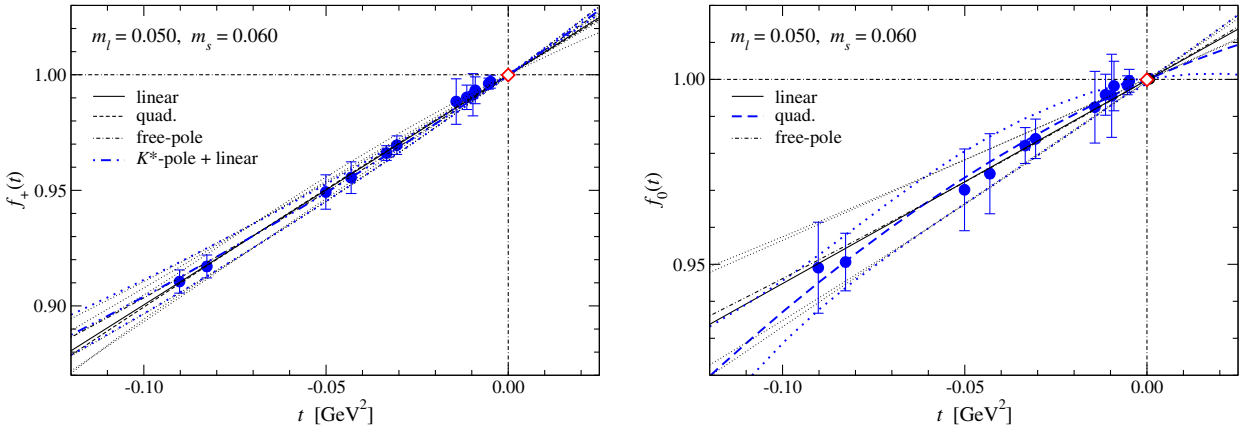

FIG. 6. Same as Fig. 4, but for $(m_l, m_s) = (0.050, 0.060)$.

$$f_+(t) = f_+(0)\left\{\frac{1}{1 - t/M_{K^*}^2} + at\right\}, \tag{25}$$

where M_{K^*} represents the strange-light vector meson mass calculated at simulation points. There could be contribution of the higher poles and cuts, which is well approximated by the additional linear term at our small values of $|t|$. We note that our data of the pion and kaon EM form factors in a similar region of t are well described by this type of the parametrization [25].

Since we simulate small values of $|t|$, our data of $f_{\{+,0\}}$ does not show any strong curvature in Figs. 4–6, and simple polynomial parametrization also describes our data well

$$f_{\{+,0\}}(t) = f_+(0)\left\{1 + \lambda'_{\{+,0\}}\frac{t}{M_{\pi^\pm,\mathrm{phys}}^2} + \lambda''_{\{+,0\}}\left(\frac{t}{M_{\pi^\pm,\mathrm{phys}}^2}\right)^2\right\} \tag{26}$$

even without the quadratic term. The conventional free-pole form

$$f_{\{+,0\}}(t) = \frac{f_{\{+,0\}}(0)}{1 - t/M_{\mathrm{pole},\{+,0\}}^2} \tag{27}$$

also works well.

In this study, we estimate $f_+(0)$ and $df_{\{+,0\}}/dt|_{t=0}$ by a simultaneous fit using the VMD-based form (25) for f_+ and the quadratic form (26) for f_0. The uncertainty due to the choice of the fitting form is estimated by testing the polynomial and free-pole forms for f_+ and the linear and free-pole forms for f_0. Fit results are summarized in Table II, where we list the phenomenologically familiar slope parameter $\lambda'_{\{+,0\}}$ in the quadratic parametrization (26) instead of $df_{\{+,0\}}/dt|_{t=0} = f_+(0)\lambda'_{\{+,0\}}/M_{\pi^\pm,\mathrm{phys}}^2$.

In the simulated region of t, all the aforementioned parametrizations describe our data well with $\chi^2/\mathrm{d.o.f} \lesssim 0.5$. The choice of the parametrization leads to small uncertainty for $f_+(0)$ compared to the statistical accuracy. For the slope parameter $\lambda'_{\{+,0\}}$, the systematic error is more important, but not so large compared to the statistical one.

TABLE II. Fit results for normalization $f_+(0)$ and slope parameters $\lambda'_{\{+,0\}}$.

m_l	m_s	$f_+(0)$	$\lambda'_+ \times 10^2$	$\lambda'_0 \times 10^2$
0.050	0.080	$0.9986(11)(^{+2}_{-1})$	2.02(7)(12)	1.10(28)(11)
0.050	0.060	0.99991(25)(−8)	2.12(14)(22)	0.84(51)(27)
0.035	0.080	0.9937(31)(+8)	2.37(11)(18)	1.42(29)(11)
0.035	0.060	$0.9977(20)(^{+4}_{-2})$	2.52(19)(19)	1.72(42)(26)
0.025	0.080	$0.9919(18)(^{+7}_{-5})$	2.51(5)(21)	1.46(17)(7)
0.025	0.060	$0.9969(46)(^{+1}_{-11})$	2.74(14)(26)	1.59(52)(18)
0.015	0.080	$0.9847(34)(^{+4}_{-5})$	2.72(10)(22)	1.70(15)(1)
0.015	0.060	$0.9922(74)(^{+18}_{-7})$	2.75(13)(32)	1.92(32)(14)

IV. CHIRAL EXTRAPOLATION OF FORM FACTORS

A. ChPT formulas and LECs

The momentum transfer and quark mass dependence of the form factors is known up to NNLO in SU(3) ChPT [19,20]. Let us denote the chiral expansion as

$$f_X(t) = f_{X,0} + f_{X,2}(t) + f_{X,4}(t) + f_{X,6}(t) \quad (X = +, -, 0), \tag{28}$$

where $f_{X,0}, f_{X,2}$, and $f_{X,4}$, represent the LO, NLO, and NNLO contributions, respectively. We add a possible higher order term $f_{X,6}$, the functional form of which is not yet known.

The current conservation fixes the normalization of the vector form factor in the chiral limit as $f_{+,0} = 1$. The NLO contribution can be decomposed into two parts

TABLE III. Input values for $O(p^4)$ couplings L_i^r at renormalization scale $\mu = M_\rho$. We use L_9^r from our study of the EM form factors [25], whereas $L_{\{1-8\}}$ are taken from a phenomenological study [51]. In that paper, authors presented two estimates obtained from different ChPT fits of experimental data. The central value and the first statistical error of $L_{\{1-8\}}$ are from the authors' preferred fit, whereas we assign the difference between the two estimates as the second systematic error.

$L_1^r \times 10^3$	$L_2^r \times 10^3$	$L_3^r \times 10^3$	$L_4^r \times 10^3$	$L_5^r \times 10^3$
0.53(6)(+11)	0.81(4)(−22)	−3.07(20)(+27)	0.3(0)(+0.46)	1.01(6)(−51)
$L_6^r \times 10^3$	$L_7^r \times 10^3$	$L_8^r \times 10^3$	$L_9^r \times 10^3$	
0.14(5)(+35)	−0.34(9)(+15)	0.47(10)(−30)	$4.6(1.1)(^{+0.1}_{-0.5})$	

$$f_{+,2}(t) = f_{+,2,L}(t) + f_{+,2,B}(t). \tag{29}$$

The first part $f_{+,2,L}$ represents the analytic term arising from the tree diagram with a vertex arising from the $O(p^4)$ chiral Lagrangian $\mathcal{L}_4$,

$$F_\pi^2 f_{+,2,L}(t) = 2L_9^r t. \tag{30}$$

Note that p symbolically represents the Nambu-Goldstone (NG) boson momentum, and L_9^r is a LEC in $\mathcal{L}_4$. This contribution does not involve quark masses to be compatible with the current conservation $f_{+,2,L}(0) = 0$.

The other part is the contribution of loop diagrams

$$F_\pi^2 f_{+,2,B}(t) = \frac{3}{8}\{\bar{A}(M_\pi^2) + 2\bar{A}(M_K^2) + \bar{A}(M_\eta^2)\} - \frac{3}{2}\{\bar{B}_{22}(M_\pi^2, M_K^2, t) + \bar{B}_{22}(M_K^2, M_\eta^2, t)\}, \tag{31}$$

where $\bar{A}$ and $\bar{B}_{22}$ represent one-loop integral functions. We refer the readers to Refs. [25,47] for their definition and expression. Note that the so-called ξ-expansion is employed in this study: the form factors are expanded in terms of $\xi_{\{\pi,K,\eta\}} = M^2_{\{\pi,K,\eta\}}/(4\pi F_\pi)^2$, where F_π represents the pion decay constant. In Ref. [48], we demonstrated that the ξ-expansion of the meson masses and decay constants has a better convergence than the expansion in terms of $m_q/(4\pi F_0)^2$. Here F_0 is the decay constant in the chiral limit. The ξ-expansion has another important advantage that ChPT formulas are free from the unknown LEC F_0.

This is also the case for the NNLO contribution

$$f_{+,4}(t) = f_{+,4,C}(t) + f_{+,4,L}(t) + f_{+,4,B}(t). \tag{32}$$

Here $f_{+,4,B}$ represents the contribution of two-loop diagrams without any vertices from $\mathcal{L}_4$ and $O(p^6)$ chiral Lagrangians $\mathcal{L}_6$ [49]. While its expression is rather lengthy [50], it does not contain any LECs in the ξ-expansion, and is not an obstacle to obtaining a stable chiral extrapolation.

The term $f_{+,4,L}$ mainly arises from the one-loop diagrams with one vertex from $\mathcal{L}_4$, and hence depends on the $O(p^4)$ couplings L_i^r. At the level of NLO, only L_9^r appears in $f_{+,2,L}$, and we fix it to an estimate obtained from our study of the EM form factors [25]. Other $L_{\{1-8\}}$ appear only in small NNLO term $f_{+,4,L}$. We fix them to a recent phenomenological estimate in Ref. [51]. These input values are listed in Table III.

The NNLO analytic term $f_{+,4,C}$ arises from tree diagrams with one vertex from $\mathcal{L}_6$. A central issue in our analysis based on NNLO ChPT is how to deal with many $O(p^6)$ couplings C_i^r appearing in this contribution

$$F_\pi^4 f_{+,4,C} = -8c^r_{+,\pi K}(M_K^2 - M_\pi^2)^2 - 4c^r_{+,\pi t}M_\pi^2 t - 4c^r_{+,Kt}M_K^2 t - 4c^r_{t^2}t^2, \tag{33}$$

where the coefficients c_X^r's are linear combinations of $O(p^6)$ couplings

$$c^r_{+,\pi K} = C^r_{12} + C^r_{34}, \tag{34}$$

$$c^r_{+,\pi t} = 2C^r_{12} + 4C^r_{13} + C^r_{64} + C^r_{65} + C^r_{90}, \tag{35}$$

$$c^r_{+,Kt} = 2C^r_{12} + 8C^r_{13} + 2C^r_{63} + 2C^r_{64} + C^r_{90}, \tag{36}$$

$$c^r_{t^2} = C^r_{88} - C^r_{90}. \tag{37}$$

Similar to the case of L_i^r, the chiral behavior of the EM form factors provides helpful information about C_i^r. The coefficient of the $O(t^2)$ term, namely $c^r_{t^2}$, is the same as the NNLO analytic term of the EM form factors

$$F_\pi^4 F^{\pi^+}_{V,4,C}(t) = -4c^r_{\pi^+,\pi t}M_\pi^2 t - 8c^r_{\pi^+,Kt}M_K^2 t - 4c^r_{t^2}t^2, \tag{38}$$

$$F_\pi^4 F^{K^+}_{V,4,C}(t) = -4c^r_{K^+,\pi t}M_\pi^2 t - 4c^r_{K^+,Kt}M_K^2 t - 4c^r_{t^2}t^2, \tag{39}$$

$$F_\pi^4 F^{K^0}_{V,4,C}(t) = -\frac{8}{3}c^r_{K^0}(M_\pi^2 - M_K^2)t, \tag{40}$$

where

$$c^r_{\pi^+,\pi t} = 4C^r_{12} + 4C^r_{13} + 2C^r_{63} + C^r_{64} + C^r_{65} + 2C^r_{90}, \tag{41}$$

$$c^r_{\pi^+,Kt} = 4C^r_{13} + C^r_{64}, \tag{42}$$

$$c^r_{K^+,\pi t} = 4C^r_{13} + \frac{2}{3}C^r_{63} + C^r_{64} - \frac{1}{3}C^r_{65}, \tag{43}$$

TABLE IV. Input values for the linear combinations of $O(p^6)$ couplings obtained in our study of EM form factors [25].

$c^r_{\pi^+,\pi t} \times 10^5$	$c^r_{\pi^+,Kt} \times 10^5$	$c^r_{l^2} \times 10^5$
$-1.95(84)(^{+38}_{-21})$	$-1.4(1.2)(^{+0.1}_{-0.7})$	$-6.4(1.1)(0.1)$

$$c^r_{K^+,Kt} = 4C^r_{12} + 8C^r_{13} + \frac{4}{3}C^r_{63} + 2C^r_{64} + \frac{4}{3}C^r_{65} + 2C^r_{90}, \tag{44}$$

$$c^r_{K^0} = 2C^r_{63} - C^r_{65}. \tag{45}$$

In addition, two coefficients for the $K \to \pi$ decays, $c^r_{+,\pi t}$ and $c^r_{+,Kt}$, are written in terms of those for the EM form factors as

$$c^r_{+,\pi t} = \frac{1}{2}(c^r_{\pi^+,\pi t} + c^r_{\pi^+,Kt} - c^r_{K^0}), \tag{46}$$

$$c^r_{+,Kt} = \frac{1}{2}(c^r_{\pi^+,\pi t} + 3c^r_{\pi^+,Kt} + c^r_{K^0}). \tag{47}$$

Therefore, we have only single free parameter $c^r_{+,\pi K}$ in our chiral extrapolation of f_+ at the level of NNLO. The term $-8c^r_{+,\pi K}(M_K^2 - M_\pi^2)^2$ in $f_{+,4,C}$ describes the SU(3) breaking effects at $t = 0$, and hence is absent in the EM form factors. The coefficient $c^r_{+,\pi K}$ is, therefore, to be determined from the data of f_+. For other coefficients $c^r_{+,\pi t}$, $c^r_{+,\pi t}$ and $c^r_{l^2}$, we use our estimate [25], which is summarized in Table IV. The uncertainty due to the choice of the input in Tables III and IV is estimated by repeating the following analysis with the input shifted by its uncertainty quoted in the tables.

The LO contribution to the other form factors are given as $f_{-,0} = 0$ and $f_{0,0} = 1$. At higher orders, however, additional LECs appear through f_-, which is absent in the EM form factors. For instance, the coefficients

$$c^r_{-,t} = -2C^r_{12} + C^r_{88} - C^r_{90}, \tag{48}$$

$$c^r_{-,\pi} = 6C^r_{12} + 4C^r_{13} + 2C^r_{15} + 4C^r_{17} + 2C^r_{34} + C^r_{64} + C^r_{65} + C^r_{90}, \tag{49}$$

$$c^r_{-,K} = 6C^r_{12} + 8C^r_{13} + 4C^r_{14} + 4C^r_{15} + 2C^r_{34} + 2C^r_{63} + 2C^r_{64} + C^r_{90} \tag{50}$$

for the NNLO analytic terms for f_-

$$f_{-,4,C} = 4c^r_{-,t}(M_K^2 - M_\pi^2)t + 4c^r_{-,\pi}(M_K^2 - M_\pi^2)M_\pi^2 + 4c^r_{-,K}(M_K^2 - M_\pi^2)M_K^2 \tag{51}$$

have C^r_{14}, C^r_{15} and C^r_{17}. The information of f_+ and the EM form factors is not so helpful in constraining them. In this study, therefore, we calculate the following quantity,

$$\tilde{f}_0(t) = f_0(t) + \frac{t}{M_K^2 - M_\pi^2}\left(1 - \frac{F_K}{F_\pi}\right), \tag{52}$$

using our data of F_K/F_π obtained in Ref. [52]. As proposed in Ref. [20], the Callan-Treiman and Dashen-Weinstein theorems [53,54],

$$f_0(M_K^2 - M_\pi^2) \sim \frac{F_K}{F_\pi}, \tag{53}$$

suggest a large cancellation between f_0 and F_K/F_π even out of the Callan-Treiman point $t = M_K^2 - M_\pi^2$. Actually, in the chiral expansion of $\tilde{f}_0$,

$$\tilde{f}_0(t) = \tilde{f}_{0,0} + \tilde{f}_{0,2}(t) + \tilde{f}_{0,4}(t) + \tilde{f}_{0,6}(t), \tag{54}$$

$$\tilde{f}_{0,2}(t) = \tilde{f}_{0,2,L}(t) + \tilde{f}_{0,2,B}(t), \tag{55}$$

$$\tilde{f}_{0,4}(t) = \tilde{f}_{0,4,C}(t) + \tilde{f}_{0,4,L}(t) + \tilde{f}_{0,4,B}(t), \tag{56}$$

the L^r_i-dependent NLO term vanishes, $\tilde{f}_{0,2,L} = 0$. The NNLO analytic term has a rather simple form,

$$\begin{aligned} F_\pi^4 \tilde{f}_{0,4,C}(t) &= -8(C^2_{12} + C^r_{34})(M_K^2 - M_\pi^2)^2 \\ &\quad + 8(2C^r_{12} + C^r_{34})(M_K^2 + M_\pi^2)t - 8C^r_{12}t^2 \\ &= -8c^r_{+,\pi K}(M_K^2 - M_\pi^2)^2 \\ &\quad + 8(C^r_{12} + c^r_{+,\pi K})(M_K^2 + M_\pi^2)t - 8C^r_{12}t^2. \end{aligned} \tag{57}$$

Genuine loop contributions, $\tilde{f}_{0,2,B}$ and $\tilde{f}_{0,4,B}$, are free from the LECs, and we use the input in Table III for L^r_i-dependent NNLO contribution $\tilde{f}_{0,4,L}$. Therefore, a simultaneous fit to f_+ and $\tilde{f}_0$ has only two fit parameters $c^r_{+,\pi K}$ and C^r_{12} (or C^r_{34}).

B. Chiral extrapolation and normalization of form factors

The Ademollo-Gatto theorem [1,2] states that SU(3) breaking effects in $f_+(t)$ is second order in $(m_s - m_l)$ at $t = 0$. The chiral expansion (28)–(37) is reduced into a simpler form with

$$f_{+,2,L}(0) = 0, \tag{58}$$

$$f_{+,2,B}(0) = \frac{3}{2}H_{K\pi} + \frac{3}{2}H_{K\eta}, \tag{59}$$

$$f_{+,4,C}(0) = -8c^r_{+,\pi K}(M_K^2 - M_\pi^2)^2, \tag{60}$$

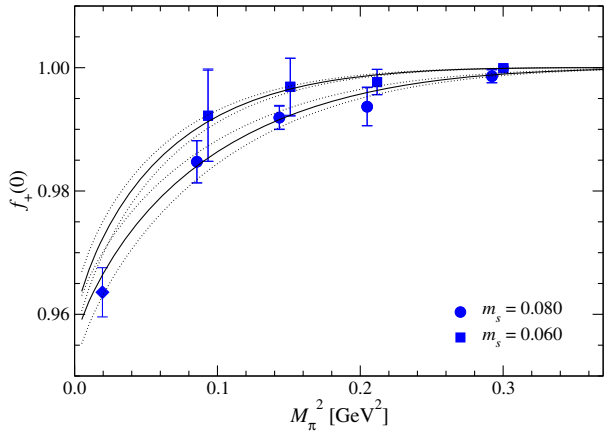

FIG. 7. Chiral extrapolation of $f_+(0)$ as a function of M_π^2. Solid circles and squares show our data at $m_s = 0.080$ and 0.060. The blue diamond is the value extrapolated to the physical point $(m_{l,\mathrm{phys}}, m_{s,\mathrm{phys}})$. We note that the physical strange quark mass $m_{s,\mathrm{phys}}$ (diamond) is slightly off the simulated values (solid lines).

where

$$H_{PQ} = -\frac{1}{128\pi^2 F_\pi^2}\left\{M_P^2 + M_Q^2 - \frac{2M_P^2 M_Q^2}{M_P^2 - M_Q^2}\ln\left[\frac{M_P^2}{M_Q^2}\right]\right\}. \tag{61}$$

In previous lattice studies, therefore, one often determines $f_+(0)$ at simulated quark masses by assuming a phenomenological parametrization of the t dependence of the form factors, and then extrapolates $f_+(0)$ to the physical point $(m_{l,\mathrm{phys}}, m_{s,\mathrm{phys}})$ based on NLO or NNLO ChPT.

We carry out this type of the conventional analysis using the data of $f_+(0)$ in Table II. As plotted in Fig. 7, the data are well described by the NNLO ChPT formula with a good value of $\chi^2/\mathrm{d.o.f.} \sim 0.2$. Numerical fit results are summarized in Table V. The value extrapolated to the physical point $(m_{l,\mathrm{phys}}, m_{s,\mathrm{phys}})$ is consistent with recent lattice estimates $f_+(0) \approx 0.97$ [8–11].

The chiral expansion has reasonable convergence $f_+(0) = 0.9636(40) = 1 - 0.0232 - 0.0132(40)$ at the physical point. However, Fig. 8 shows that the NLO and NNLO contributions, $f_{+,2}(0)$ and $f_{+,4}(0)$, are comparable at unphysically heavy $M_\pi \sim 300$–500 MeV, and there is a significant cancellation between the analytic $(f_{+,4,C}(0))$ and nonanalytic $(f_{+,4,L}(0)$ and $f_{+,4,B}(0))$ NNLO contributions.

In order to estimate the systematic error due to neglected higher order corrections, we also test a fitting form including a N^{3}LO analytic term $f_{+,6} = d_+ M_\pi^2 (M_K^2 - M_\pi^2)^2/F_\pi^6$, where the factor $(M_K^2 - M_\pi^2)^2$ is motivated by the Ademollo-Gatto theorem. However, the coefficient $d_+ = -1.1(1.6) \times 10^6$ is poorly determined, and the extrapolated value $f_+(0) = 0.971(13)$ is statistically consistent with that from the NNLO fit. This observation and the good value of $\chi^2/\mathrm{d.o.f.}$ for the NNLO fit suggest that the uncertainty due to the truncation of the chiral expansion at NNLO is not large compared to the statistical accuracy. We treat the difference in $f_+(0)$ between the fits with and without the N^{3}LO term as a systematic uncertainty in Table V.

We can examine the significance of the higher order correction without assuming the form of $f_{+,6}$. Let us consider a quantity

$$\Delta f(0) = f_+(0) - f_{+,0} - f_{+,2,L}(0) - f_{+,2,B}(0) - f_{+,4,L}(0) - f_{+,4,B}(0), \tag{62}$$

which is the sum of the NNLO analytic term and the possible higher order correction $f_{+,4,C}(0) + f_{+,6}(0)$. Note that $f_{+,0}(0)$, $f_{+,2,B}(0)$ and $f_{+,4,B}(0)$ are LEC-free in ξ-expansion, and hence Δf can be calculated from our data of $f_+(0)$ and inputs in Tables III. We can define an effective value of $c^r_{+,\pi K} = C^r_{12} + C^r_{34}$ as

$$c^r_{+,\pi\mathrm{K,eff}} = -\frac{F_\pi^4}{8(M_K^2 - M_\pi^2)^2}\Delta f = c^r_{+,\pi K} + O(M_\pi^2, M_K^2), \tag{63}$$

which deviates from $c^r_{+,\pi K}$ and shows a nontrivial quark mass dependence, if the higher order correction $f_{+,6}$ is significant in the simulation region. As shown in Fig. 9, however, our result has small dependence on m_l and m_s suggesting that the higher order correction is not large compared to the statistical accuracy.

TABLE V. Numerical results of NNLO ChPT fits to form factors. The first line shows results of the conventional fit to $f_+(0)$ in terms of the NG boson masses $M^2_{\{\pi,K\}}$. The second (third) line is from the fit to $f_+(t)$ ($f_+(t)$ and $\tilde{f}_0(t)$) in terms of $M^2_{\{\pi,K\}}$ and t. The first error is statistical. The second and third are systematics due to the choice of the input L^r_i, and truncation of the chiral expansion at NNLO. Note $c^r_{+,\pi K} = C^r_{12} + C^r_{34}$ (Eq. (34)).

fit data	$f_+(0)$	$c^r_{+,\pi K} \times 10^5$	$C^r_{12} \times 10^5$	$C^r_{34} \times 10^5$
$f_+(0)$	$0.9636(40)(^{+42}_{-6})(+79)$	$0.53(7)(-6)(-17)$	–	–
$f_+(t)$	$0.9691(42)(^{+45}_{-5})(-45)$	$0.429(73)(^{+5}_{-71})(+90)$	–	–
$f_+(t)$, $\tilde{f}_0(t)$	$0.9636(36)(^{+41}_{-4})(^{+28}_{-19})$	$0.524(62)(^{+1}_{-80})(^{+33}_{-58})$	$-0.23(7)(^{+34}_{-13})(^{+5}_{-93})$	$0.76(11)(^{+9}_{-42})(^{+95}_{-11})$

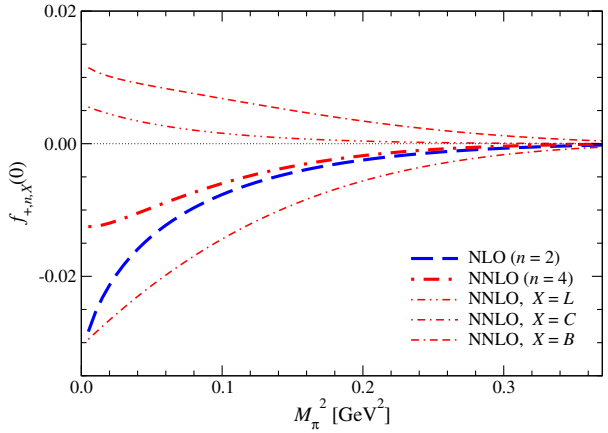

FIG. 8. LEC-(in)dependent NLO and NNLO contributions to $f_+(0)$. Thick dashed and dot-dashed lines are the NLO and NNLO contributions, whereas the NNLO terms, $f_{+,4,L}(0)$, $f_{+,4,C}(0)$ and $f_{+,4,B}(0)$, are plotted by the thin dot-dot-dashed, dot-dashed and dot-dashed-dashed lines, respectively.

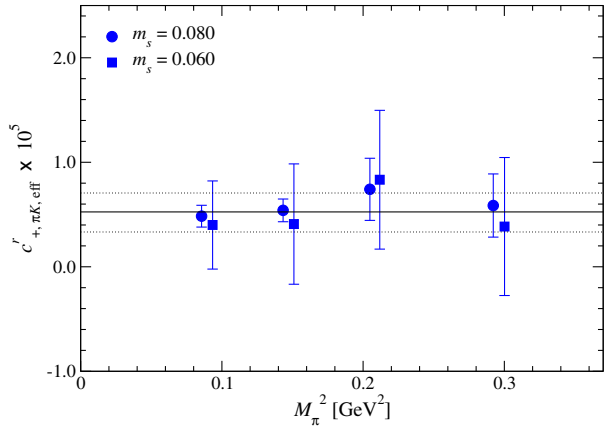

FIG. 9. Effective value $c^r_{+,\pi\mathrm{K,eff}}$ as a function of M_π^2. Squares are slightly shifted along the horizontal axis for clarity. The solid and dotted lines show $c^r_{+,\pi K}$ obtained from the NNLO chiral fit and its uncertainty.

It is advantageous to use not only $f_+(0)$ but all the data of $f_+(t)$ to better constrain the possible higher order chiral corrections. Parametrizing both the t and quark mass dependences based on ChPT reduces the model dependence of our analysis. We, therefore, carry out a fit for $f_+(t)$ using the chiral expansion (28) as a function of t, M_π^2 and M_K^2. As shown in Fig. 10, the t dependence of our data is also described well by the NNLO formula with an acceptable value of $\chi/\mathrm{dof} \sim 0.7$, because we simulate a limited region of $t \sim 0$.

Results for the LEC $c^r_{+,\pi K}$ and the normalization $f_+(0)$ at the physical point in Table V show good consistency with those from the conventional analysis. Their systematic error due to the truncation of the chiral expansion at NNLO is estimated by repeating the fit with each of the following higher order terms

$$F_\pi^6 f_{+,6} = d_+ M_\pi^2 (M_K^2 - M_\pi^2)^2, \quad d_+ M_\pi^4 t, \quad d_+ M_\pi^2 t^2, \quad d_+ M_\pi^2 M_K^2 t. \tag{64}$$

This uncertainty is slightly smaller than the conventional analysis, because the coefficient d_+ is better constrained with more data at nonzero t's.

In order to make use of all the available data, we performed a simultaneous fit to $f_+(t)$ and $\tilde{f}_0(t)$ as a function of t, M_π^2 and M_K^2. As shown in Fig. 11, the NNLO formulas (28) and (54) describe our data well with a good value of $\chi^2/\mathrm{d.o.f.} \sim 0.7$. Numerical results of the fit are summarized in Table V. We estimate the uncertainty due to possible higher order corrections by testing the N^{3}LO terms (64) for $f_{+,6}$ and the followings for $\tilde{f}_{0,6}$

$$F_\pi^6 \tilde{f}_{0,6} = d_+ M_\pi^2 (M_K^2 - M_\pi^2)^2, \quad d_0 M_\pi^4 t, \quad d_0 M_\pi^2 t^2, \quad d_0 M_\pi^2 M_K^2 t. \tag{65}$$

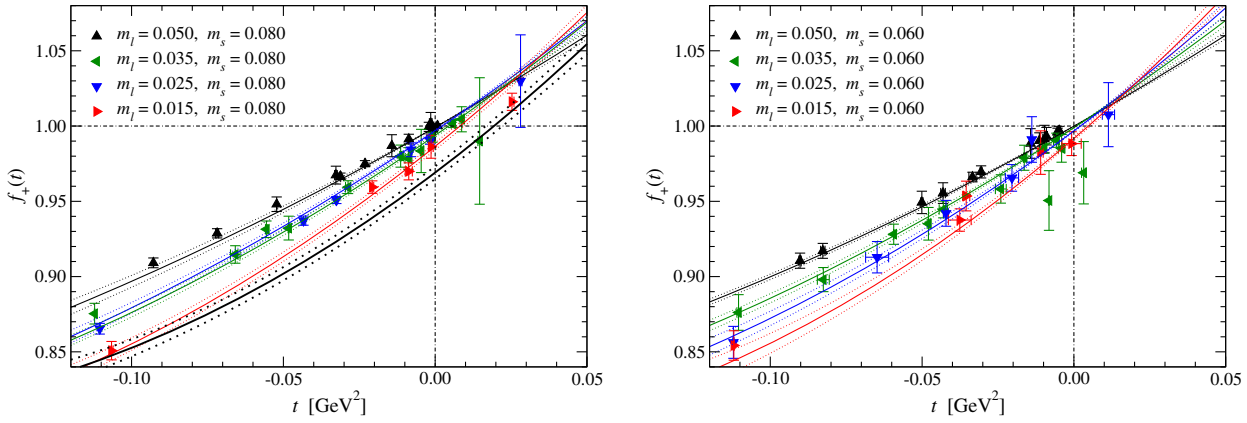

FIG. 10. Chiral extrapolation of $f_+(t)$ as a function of t. Different symbols show data at different values of m_l, whereas the left and right panels are for $m_s = 0.080$ and 0.060, respectively. Thin solid and dotted lines show the fit curve and its statistical uncertainty. We also plot those at the physical point $(m_{l,\mathrm{phys}}, m_{s,\mathrm{phys}})$ by thick lines in the left panel at $m_s \sim m_{s,\mathrm{phys}}$.

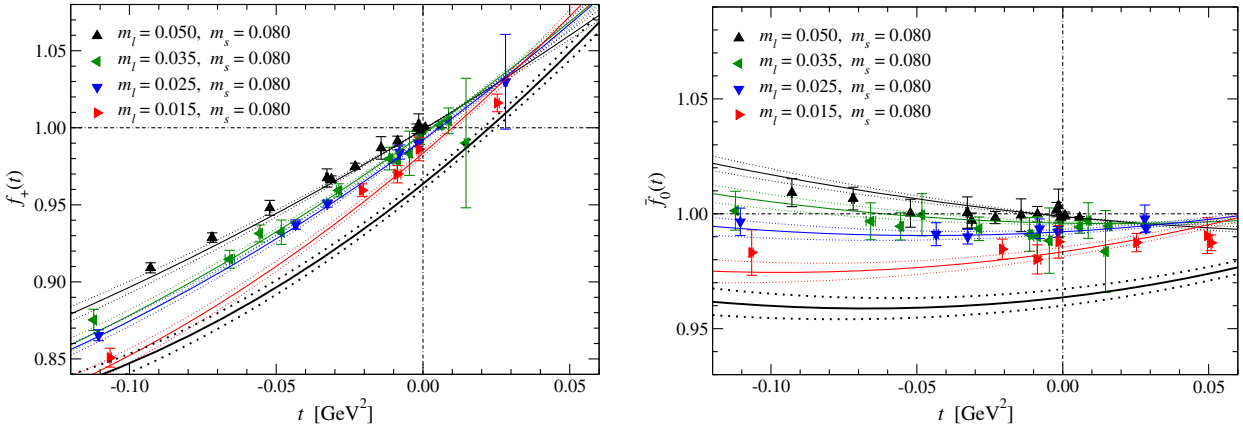

FIG. 11. Simultaneous chiral fit to $f_+(t)$ (left panel) and $\tilde{f}_0(t)$ (right panel) at $m_s = 0.080$. Data at different values of m_l are plotted by different symbols as a function of t. Thin solid and dotted line shows the fit curve and the statistical uncertainty, whereas thick lines show those at $(m_{l,\mathrm{phys}}, m_{s,\mathrm{phys}})$.

Table V shows good consistency in $c^r_{+,\pi K}$ and $f_+(0)$ at the physical point among the three types of the chiral fit: namely, the fit to $f_+(0)$, that to $f_+(t)$, and the simultaneous fit to $f_+(t)$ and $\tilde{f}_0(t)$. This is also demonstrated in Fig. 12, where the M_π dependence of $f_+(0)$ at $m_s = 0.080 \sim m_{s,\mathrm{phys}}$ is reproduced from the three fits. We observe good agreement within $\sim 1\sigma$ in the whole simulation region of M_π^2.

Table V shows that the statistical accuracy of the fit results is not largely different between the conventional fit and the fit to f_+. Indeed, these two fits use the same data of f_+ but different parametrizations for the t dependence: Eq. (25) or ChPT. The statistical error is slightly reduced by using $\tilde{f}_0$. The uncertainty due to the choice of the input (Tables III and IV) is more or less the same among the three fits. However, the uncertainty due to the truncation of the chiral expansion is significantly reduced by including more data into the ChPT fit. From this observation, we consider the simultaneous fit to f_+ and $\tilde{f}_0$ as our best fit.

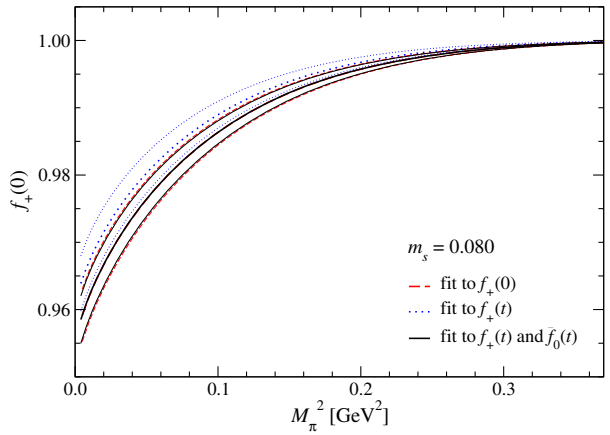

FIG. 12. Comparison of fit curves for $f_+(0)$ at $m_s = 0.080 \sim m_{s,\mathrm{phys}}$. The dashed, dotted and solid lines lines are reproduced from the fits to $f_+(0)$, $f_+(t)$ and the simultaneous fit to $f_+(t)$ and $\tilde{f}_0(t)$, respectively. For each fit, the thick line shows the central value, whereas its statistical error is shown by the two thin lines.

We investigate the convergence of this best fit in Fig. 13. Our observations on f_+ at large spacelike momentum transfer $-t \gg 0$ are similar to those on the charged meson EM form factors $F_V^{\{\pi^+,K^+\}}$ in Ref. [25]. The analytic term $f_{+,2,L}$ ($f_{+,4,C}$) is dominant NLO (largest NNLO) contribution to $f_{+,2}$ ($f_{+,4}$). We note that our estimate of the relevant LECs in Tables III–V is not unexpectedly large, and consistent with an order estimate [51]

$$L_i^r = O((4\pi)^{-2}) = O(6 \times 10^{-3}),$$
$$C_i^r = O((4\pi)^{-4}) = O(4 \times 10^{-5}). \tag{66}$$

The large analytic terms, $f_{+,2,L}$ and $f_{+,4,C}$, suggest the importance of the first-principle determination of the relevant LECs. While we employ the input in Table III for other LECs involved in $f_{+,4,L}$, this term turns out to be small. Therefore, the systematic uncertainty due to the choice of the input is not large.

The convergence at $-t \gg 0$ is reasonably good and becomes better toward smaller M_π. This is because the dominant NLO term $f_{+,2,L} \propto t/F_\pi^2$ is not suppressed by the NG boson masses and even enhanced by the factor F_π^{-2} in the ξ-expansion. A similar convergence property is also observed for the EM form factors $F_V^{\{\pi^+,K^+\}}$ [25].

There is a property of f_+ different from $F_V^{\{\pi^+,K^+\}}$ near the important reference point $t = 0$. Unless $m_l \neq m_s$, each chiral correction does not necessarily vanish except $f_{+,2,L}$, which is dominantly large at $-t \gg 0$ (blue thin dashed lines in Fig. 13). As a result, the chiral expansion has a poorer convergence towards $t = 0$ as already observed in Fig. 8. Note, however, that our analysis in Fig. 9 does not suggest statistically significant N^{3}LO nor higher order corrections.

In our analysis, the quantity $\tilde{f}_0$ is used to obtain additional constraints on the relevant $O(p^6)$ couplings, C_{12}^r and

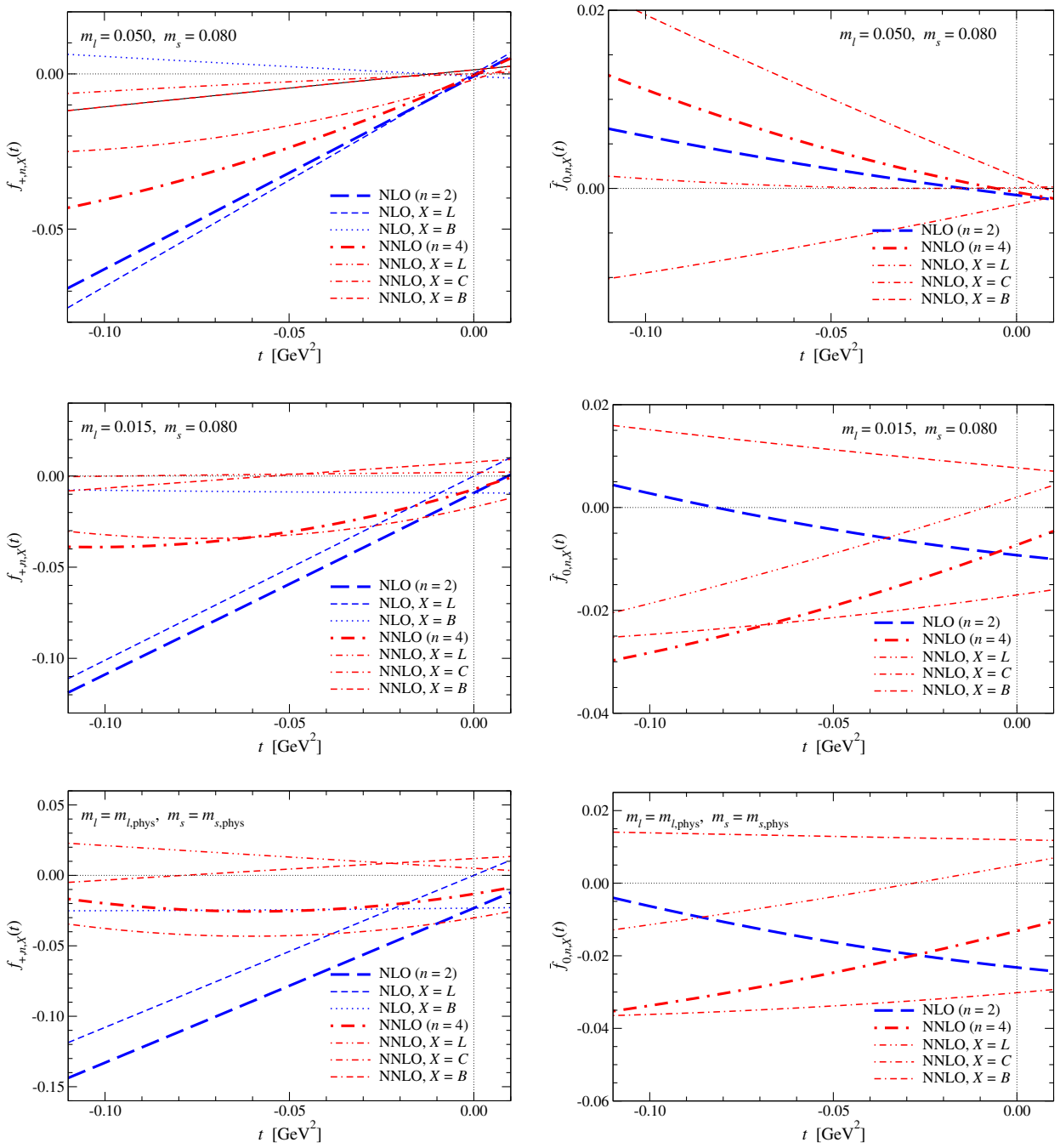

FIG. 13. LEC-(in)dependent NLO and NNLO contributions to $f_+(t)$ (left panels) and $\tilde{f}_0(t)$ (right panels) as a function of t. The top, middle and bottom panels show data at $(m_l, m_s) = (0.050, 0.080)$, (0.015,0.080) and the physical point $(m_{l,\mathrm{phys}}, m_{s,\mathrm{phys}})$, respectively. The net NLO and NNLO contributions are plotted by thick blue dashed and red dot-dashed lines, respectively. Thin lines show their breakdown into LEC-(in)dependent terms.

C^r_{34}. For this purpose, $\tilde{f}_0$ is designed to have no NLO analytic term, which is a dominant contribution to f_+, and its dependence on L^r_i starts from NNLO. The right panels of Fig. 13 show that the L_i-dependent NNLO correction $\tilde{f}_{0,4,L}$ is not large with our choice of the input in Table III. The remaining loop corrections, $\tilde{f}_{0,2,B}$ and $\tilde{f}_{0,4,B}$, are parameter free in the ξ-expansion. Therefore, $\tilde{f}_0$ has reasonable sensitivity to the NNLO analytic term $\tilde{f}_{0,4,C}$. This leads to our observation in Table V: incorporating $\tilde{f}_0$ into the chiral extrapolation is helpful in improving the statistical accuracy of $c^r_{+,\pi K}$ and $f_+(0)$, and also in reducing their systematic error due to the truncation of the chiral expansion.

For phenomenological applications, it is preferable to separately fix C^r_{12} and C^r_{34} rather than their sum $c^r_{+,\pi K}$. This

is only possible with the data of $\tilde{f}_0$ by disentangle their M_π^2, M_K^2 and t dependences in the NNLO correction (57). As mentioned above, however, $\tilde{f}_0$ is designed to have the small NLO correction $\tilde{f}_{0,2}$. This quantity is sensitive to not only NNLO but the even higher order corrections (64) and (65) added by hand to estimate the systematic uncertainty due to the truncation of the chiral expansion. As a result, this uncertainty for C_{12}^r and C_{34}^r is rather large in Table V. In this study, therefore, we only confirm that our results are consistent with the order estimate (66). We note that a better determination of C_{12}^r and C_{34}^r needs more data of $\tilde{f}_0$ at smaller values of M_π and M_K.

C. Form factor shape

In order to support the reliability of the determination of $f_+(0)$ with the subpercent-level accuracy, it is important to check the consistency of the form factors' shape on the lattice with experiments. In recent analyses of experimental data, it is popular to employ the so-called dispersive parametrization of the t dependence [16,17] based on the analyticity of the form factors. In this study, however, we consider the slope $\lambda'_{\{+,0\}}$ in the conventional quadratic parametrization (26). These are convenient in our analysis based on ChPT, since the chiral expansion is the expansion in terms of t (and the NG boson masses). We note that the quadratic parametrization has been also well studied phenomenologically and experimentally. Its relation to the dispersive one has been established [16]. From recent experimental data [3], the slopes are estimated as

$$\lambda'_+ = 2.58(7) \times 10^{-2}, \qquad \lambda'_0 = 1.36(7) \times 10^{-2}. \quad (67)$$

In this paper, we treat $M_{\pi^\pm}^2$ in Eq. (26) just as the normalization factor to make $\lambda_{\{+,0\}}$ dimensionless, and fix it to its physical value. The slope is then given as

$$\lambda'_{\{+,0\}} = \frac{M_{\pi^\pm,\mathrm{phys}}^2}{f_{\{+,0\}}(0)} \left.\frac{df_{\{+,0\}}(t)}{dt}\right|_{t=0}. \quad (68)$$

We evaluate both the normalization $f_+(0) = f_0(0)$ (Table V) and derivatives $df_{\{+,0\}}/dt|_{t=0}$ from our chiral fit of f_+ and $\tilde{f}_0$ based on NNLO ChPT.

It is straightforward to calculate $df_+/dt|_{t=0}$. From the chiral expansion (28), (29) and (32), it is given as

$$\frac{df_+(t)}{dt} = \frac{df_{+,2}(t)}{dt} + \frac{df_{+,4}(t)}{dt} + \frac{df_{+,6}(t)}{dt}, \quad (69)$$

$$\frac{df_{+,2}(t)}{dt} = \frac{df_{+,2,L}(t)}{dt} + \frac{df_{+,2,B}(t)}{dt}, \quad (70)$$

$$\frac{df_{+,4}(t)}{dt} = \frac{df_{+,4,C}(t)}{dt} + \frac{df_{+,4,L}(t)}{dt} + \frac{df_{+,4,B}(t)}{dt}. \quad (71)$$

The derivatives of $f_{+,2,L}$, $f_{+,2,B}$, $f_{+,4,C}$ and $f_{+,6}$ are analytically calculable from their expressions (30), (31), (33) and (64). Since the NNLO nonanalytic terms, $f_{+,4,L}$ and $f_{+,4,B}$, have rather lengthy expressions, we numerically evaluate their derivatives as in our study of the light meson charge radii [25].

We evaluate $df_0/dt|_{t=0}$ through

$$\frac{df_0(t)}{dt} = \frac{d\tilde{f}_0(t)}{dt} - \frac{1}{M_K^2 - M_\pi^2}\left(1 - \frac{F_K}{F_\pi}\right). \quad (72)$$

Here $d\tilde{f}_0/dt|_{t=0}$ is calculated in a similar way to $df_+/dt|_{t=0}$, whereas F_K/F_π is estimated from our NNLO chiral fit in Ref. [52].

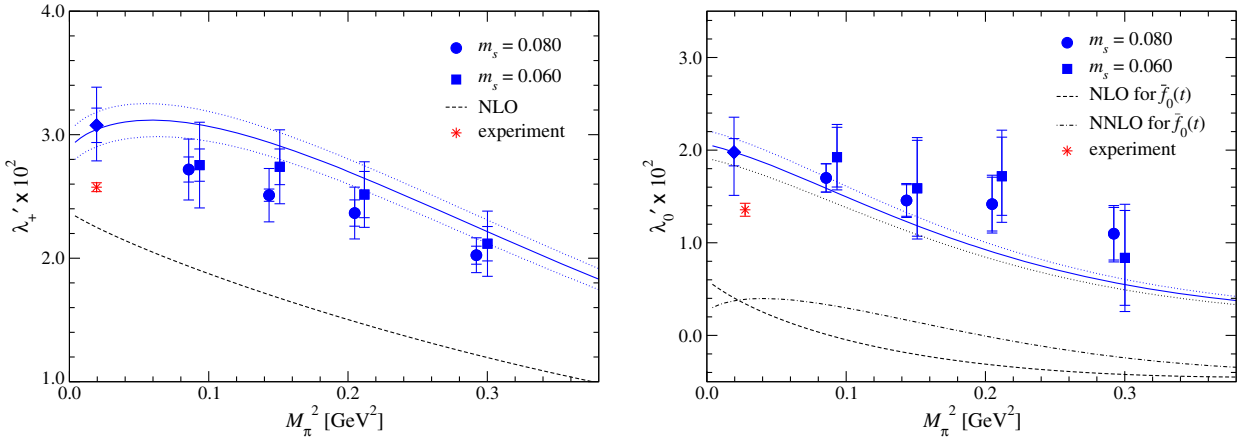

FIG. 14. Slope parameters λ'_+ (left panel) and λ'_0 (right panel) as a function of M_π^2. The blue solid and dotted lines are reproduced from our chiral fit based on NNLO ChPT, and represent the slopes at a simulated strange quark mass $m_s = 0.080$. The black dashed (dot-dashed) line shows the contribution from the NLO (NNLO) correction to f_+ and $\tilde{f}_0$. The value extrapolated to the physical point $(m_{ud,\mathrm{phys}}, m_{s,\mathrm{phys}})$ is plotted by the blue diamonds, whereas the red stars represent the experimental values (67). We also plot the values in Table II by blue circles ($m_s = 0.080$) and squares (0.060).

Our results for $\lambda'_{\{+,0\}}$ are plotted in Fig. 14 as a function of M_π^2. We observe reasonable agreement with the values in Table II, which are estimated by assuming the VMD-based parametrization (25) for f_+ and the quadratic form (26) for f_0. This agreement does not necessarily hold, since the nonanalytic chiral behavior is not explicitly taken into account in the model assumptions. The reasonable consistency in λ'_+ is, therefore, compatible with our observation in Fig. 13 that nonanalytic corrections to f_+ are not large at the simulation points.

The dashed line in the left panel of Fig. 14 shows λ'_+ up to NLO. The NNLO correction turns out to be significant at the simulation points and down to the physical point. In the whole region, the analytic term $f_{+,4,C}$ gives rise to a dominant part of the NNLO correction suggesting the importance of the first-principle determination of the relevant LECs. We observe that contribution from the NNLO nonanalytic term $f_{+,4,L}$ become significant below the simulation points $M_\pi \lesssim 0.09$ GeV^2 and leads to the nonmonotonous M_π^2 dependence of λ'_+. It is, therefore, important to study the form factor shape by taking account of the chiral logarithmic terms.

In the right panel of Fig. 14, dashed and dot-dashed lines show contributions to λ'_0 from $\tilde{f}_0$, which are not large. The slope is, therefore, dominated by the second term in the right-hand side of Eq. (72). This is because a large part of the NLO and NNLO analytic terms, which give rise to a large contribution to λ'_+, are absorbed into the second term. This suggests that a modified version [14] of the Dashen-Weinstein relation [54]

$$\frac{f_0'(0)}{f_0(0)} = \frac{\lambda'_0}{M^2_{\pi^\pm,\mathrm{phys}}} \sim \frac{1}{M_K^2 - M_\pi^2}\left(\frac{F_K}{F_\pi} - 1\right) \tag{73}$$

holds reasonably well in a wide region of $M_\pi \lesssim 500$ MeV.

D. Numerical results for form factors and LEC

Our numerical result for the normalization is

$$f_+(0) = 0.9636(36)_{\mathrm{stat}}\left(^{+49}_{-19}\right)_{\mathrm{chiral}}(29)_{a\neq 0}. \tag{74}$$

The first error is statistical. The second error is due to the chiral extrapolation and is a quadrature sum of the uncertainties from the choice of the input $L_{\{1,\ldots,8\}}$ (Table III) and the truncation of the chiral expansion at NNLO. The third one represents discretization errors at our finite lattice spacing. Since the LO term $f_{+,0} = 1$ is fixed from symmetry, we assign discretization errors to the nontrivial chiral correction $f_{+,2} + f_{+,4}$ by an order counting $O((a\Lambda_{\mathrm{QCD}})^2) \sim 8\%$ with $\Lambda_{\mathrm{QCD}} = 500$ MeV. We expect that $f_{+,2} + f_{+,4}$ also receives finite volume effects of $O(e^{-M_\pi L}) \sim 1\%$–2%. This is, however, well below other uncertainties. As shown in Fig. 15, recent lattice estimates [8–11] are consistent with our result.

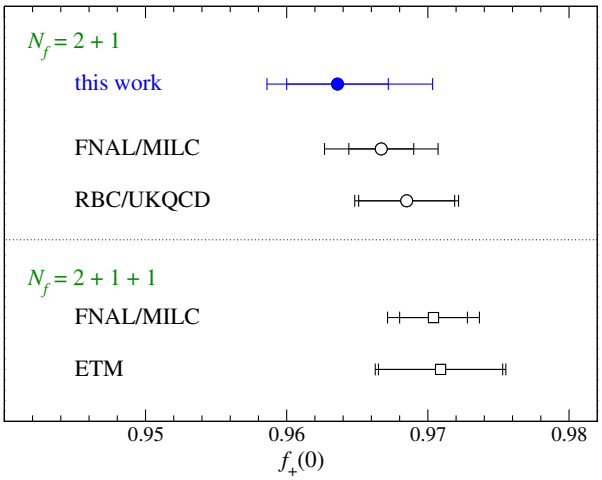

FIG. 15. Comparison of recent lattice estimates of $f_+(0)$. The filled circle shows our result (74). Recent results in $N_f = 2+1$ [8,9]. and $2+1+1$ [10,11] QCD are plotted by open circles and squares, respectively.

A latest analysis of available experimental data together with analytic calculations of the isospin and EM corrections [3,55–57] obtains $|V_{us}| f_+(0) = 0.21654(41)$ [3]. Our results lead to

$$|V_{us}| = 0.2247\left(^{+16}_{-12}\right)_{\mathrm{th}}(4)_{\mathrm{ex}}, \tag{75}$$

and a measure of the unitarity violation in the first row

$$\Delta_{\mathrm{CKM}} = |V_{ud}|^2 + |V_{us}|^2 + |V_{ub}|^2 - 1 = -0.0004\left(^{+7}_{-8}\right). \tag{76}$$

Here we use recent estimate $|V_{ud}| = 0.97420(21)$ [58] from the super-allowed nuclear β decays. Note that $|V_{ub}| \approx 4 \times 10^{-3}$ [59] is too small to affect this test of CKM unitarity, and the long-standing tension between the exclusive and inclusive decays does not change Δ_{CKM} significantly. CKM unitarity fulfilled at the level of $O(0.1\%)$ may have sensitivity to new physics at the TeV scale [60].

For the LEC and form factor shape, we obtain

$$\begin{aligned} c^r_{+,\pi K}(M_\rho) &= C^r_{12}(M_\rho) + C^r_{34}(M_\rho) \\ &= 0.524(62)_{\mathrm{stat}}\left(^{+33}_{-99}\right)_{\mathrm{chiral}}(42)_{a\neq 0} \times 10^{-5}, \end{aligned} \tag{77}$$

$$\lambda'_+ = 3.08(14)_{\mathrm{stat}}\left(^{+12}_{-4}\right)_{\mathrm{chiral}}(25)_{a\neq 0} \times 10^{-2}, \tag{78}$$

$$\lambda'_0 = 1.98(15)_{\mathrm{stat}}\left(^{+31}_{-41}\right)_{\mathrm{chiral}}(16)_{a\neq 0} \times 10^{-2}, \tag{79}$$

where we assign $O((a\Lambda_{\mathrm{QCD}})^2)$ discretization errors, and 1%–2% finite volume effects are well below other uncertainties. We note that our chiral fit to $f_+(0)$ and that to $f_+(t)$ yield consistent results for the normalization and LEC. Recent lattice estimate [8–11] and the current world

average [5] for $f_+(0)$ are in good agreement with our result. We also observe reasonable consistency with a previous lattice estimate of the LEC $c^r_{+,\pi K}(M_\rho) = 0.46(10) \times 10^{-5}$ [8] and experimental results for the slopes (67).

V. CONCLUSIONS

In this article, we have presented our study of the chiral behavior of the $K \to \pi$ semileptonic form factors. Relevant meson correlators are precisely calculated by using the all-to-all quark propagator. Our data of the form factors are directly compared with NNLO ChPT in the continuum limit by exploiting exact chiral symmetry preserved by the overlap quark action.

Similar to our observation in our study of the EM form factors, the nontrivial chiral correction to the vector form factor $f_+ - 1$ is largely dominated by the NLO analytic term $f_{+,2,L} \propto t$. As a result, the NNLO chiral expansion exhibits reasonably good convergence particularly at $t \ll 0$, and describes our data reasonably well. While $f_{+,2,L}$ vanishes and the convergence becomes poorer towards $t = 0$, our analysis suggests that N^{3}LO and even higher order corrections are not large compared to the statistical accuracy.

We determined the normalization $f_+(0)$ within $\leq 1\%$ accuracy from our chiral fit to $f_+(t)$ and $\tilde{f}_0(t)$ based on NNLO ChPT. The result is nicely consistent with CKM unitarity in the first row. We also estimate the relevant $O(p^6)$ coupling $C^r_{12} + C^r_{34}$ and the slope parameters $\lambda'_{\{+,0\}}$ from the same fit, and observe reasonable consistency with a previous lattice study and experiments, respectively.

The statistical and systematic uncertainties of $f_+(0)$ turn out to be comparable to each other with our simulation setup. Its accuracy can be improved in the future by more realistic simulations with higher statistics. Note that the uncertainty of the isospin breaking and EM corrections are typically 0.1%–0.2%. Good control of these corrections will be increasingly important, as the accuracy of $f_+(0)$ approaches this level.

Towards the continuum limit and the physical point, the computational cost of the low-lying modes rapidly increases, since the number of the necessary modes and the computational cost of the Dirac operator multiplication are both expected to scale as $\propto N_s^3 N_t$. While it is possible to add another lattice spacing or lighter pion mass on currently available computers, it is better in the long term to pursue a more realistic calculation of the kaon form factors and extension to heavy meson decays with a computationally inexpensive fermion formulation. We have carried out a comparative study of such formulations with good chiral symmetry [61], and simulations on finer lattices are underway [62]. Preliminary results have been reported for the D and B meson decay constants [63] and the $D \to \pi$ and $D \to K$ form factors [64].

ACKNOWLEDGMENTS

We thank Johan Bijnens for making his code to calculate the form factors in NNLO SU(3) ChPT available to us. Numerical simulations were performed on Hitachi SR16000 and IBM System Blue Gene Solution at High Energy Accelerator Research Organization (KEK) under support of its Large Scale Simulation Program (No. 16/17-14), and on SR16000 at YITP in Kyoto University. This work is supported, in part, by JSPS KAKENHI Grant No. JP25800147, No. JP26400259, and No. JP16H03978 and by the Ministry of Education, Culture, Sports, Science and Technology as "Priority Issue on Post-K Computer" (Elucidation of the Fundamental Laws and Evolution of the Universe) and Joint Institute for Computational Fundamental Science.

[1] R. E. Behrends and A. Sirlin, Phys. Rev. Lett. **4**, 186 (1960).
[2] M. Ademollo and R. Gatto, Phys. Rev. Lett. **13**, 264 (1964).
[3] M. Moulson, *Proc. Sci.*, CKM2016 (2017) 033, [arXiv:1704.04104].
[4] T. Kaneko, X.-R. Lyu, and A. Oyanguren, *Proc. Sci.*, CKM2016 (2017) 014, [arXiv:1705.05975].
[5] S. Aoki *et al.* (Flavor Lattice Averaging Group Collaboration), Eur. Phys. J. C **77**, 112 (2017).
[6] S. Simula, *Proc. Sci.*, CKM2016 (2017) 032, [arXiv:1704.00510].
[7] P. F. Bedaque, Phys. Lett. B **593**, 82 (2004).
[8] A. Bazavov *et al.* (Fermilab Lattice and MILC Collaborations), Phys. Rev. D **87**, 073012 (2013).
[9] P. A. Boyle *et al.* (RBC/UKQCD Collaboration), J. High Energy Phys. 06 (2015) 164.
[10] A. Bazavov *et al.* (Fermilab Lattice and MILC Collaborations), Phys. Rev. Lett. **112**, 112001 (2014).
[11] N. Carrasco, P. Lami, V. Lubicz, L. Riggio, S. Simula, and C. Tarantino, Phys. Rev. D **93**, 114512 (2016).
[12] J. Gasser and H. Leutwyler, Ann. Phys. (N.Y.) **158**, 142 (1984).
[13] J. Gasser and H. Leutwyler, Nucl. Phys. **B250**, 465 (1985).
[14] J. Gasser and H. Leutwyler, Nucl. Phys. **B250**, 517 (1985).
[15] C. Bourrely, B. Machet, and E. de Rafael, Nucl. Phys. **B189**, 157 (1981).

[16] V. Bernard, M. Oertel, E. Passemar, and J. Stern, Phys. Rev. D **80**, 034034 (2009).
[17] V. Bernard, M. Oertel, E. Passemar, and J. Stern, Phys. Lett. B **638**, 480 (2006).
[18] S. Aoki *et al.* (JLQCD and TWQCD Collaborations), Prog. Theor. Exp. Phys. **2012**, 01A106 (2012).
[19] P. Post and K. Schilcher, Eur. Phys. J. C **25**, 427 (2002).
[20] J. Bijnens and P.Talavera, Nucl. Phys. **B669**, 341 (2003).
[21] G. S. Bali, H. Neff, T. Düssel, T. Lippert, and K. Schilling (SESAM Collaboration), Phys. Rev. D **71**, 114513 (2005).
[22] J. Foley, K. J. Juge, A. Ó Cais, M. Peardon, S. M. Ryan, and J.-I. Skullerud (TrinLat Collaboration), Comput. Phys. Commun. **172**, 145 (2005).
[23] A. Hasenfratz, R. Hoffmann, and S. Schaefer, Phys. Rev. D **78**, 014515 (2008).
[24] T. DeGrand, Phys. Rev. D **78**, 117504 (2008).
[25] S. Aoki, G. Cossu, X. Feng, S. Hashimoto, T. Kaneko, J. Noaki, and T. Onogi (JLQCD Collaboration), Phys. Rev. D **93**, 034504 (2016).
[26] T. Kaneko *et al.* (JLQCD Collaboration), *Proc. Sci.*, LATTICE2010 (2011) 146, [arXiv:1012.0137].
[27] T. Kaneko *et al.* (JLQCD Collaboration), *Proc. Sci.*, Lattice2011 (2012) 284, [arXiv:1112.5259].
[28] T. Kaneko *et al.* (JLQCD Collaboration), *Proc. Sci.*, Lattice2012 (2012) 111, [arXiv:1211.6180].
[29] T. Kaneko *et al.* (JLQCD Collaboration), *Proc. Sci.*, LATTICE2015 (2016) 325, [arXiv:1601.07658].
[30] R. Narayanan and H. Neuberger, Nucl. Phys. **B443**, 305 (1995).
[31] H. Neuberger, Phys. Lett. B **417**, 141 (1998); **427**, 353 (1998).
[32] S. Aoki *et al.* (JLQCD Collaboration), Phys. Rev. D **78**, 014508 (2008).
[33] Y. Iwasaki, arXiv:1111.7054.
[34] P. M. Vranas, Phys. Rev. D **74**, 034512 (2006).
[35] H. Fukaya, S. Hashimoto, K.-I. Ishikawa, T. Kaneko, H. Matsufuru, T. Onogi, and N. Yamada (JLQCD Collaboration), Phys. Rev. D **74**, 094505 (2006).
[36] S. Aoki, H. Fukaya, S. Hashimoto, and T. Onogi, Phys. Rev. D **76**, 054508 (2007).
[37] S. Aoki *et al.* (JLQCD and TWQCD Collaborations), Phys. Rev. D **80**, 034508 (2009).
[38] S. Aoki *et al.* (JLQCD and TWQCD Collaborations), Phys. Lett. B **665**, 294 (2008).
[39] S.-J. Dong and K.-F. Liu, Phys. Lett. B **328**, 130 (1994).
[40] S. Hashimoto, A. X. El-Khadra, A. S. Kronfeld, P. B. Mackenzie, S. M. Ryan, and J. N. Simone, Phys. Rev. D **61**, 014502 (1999).
[41] D. Bećirević, G. Isidori, V. Lubicz, G. Martinelli, F. Mescia, S. Simula, C. Tarantino, and G. Villadoro, Nucl. Phys. **B705**, 339 (2005).
[42] N. Tsutsui *et al.* (JLQCD Collaboration), *Proc. Sci.*, LAT2005 (2005) 357, [arXiv:hep-lat/0510068].
[43] C. Dawson, T. Izubuchi, T. Kaneko, S. Sasaki, and A. Soni (RBC Collaboration), Phys. Rev. D **74**, 114502 (2006).
[44] J. Bijnens and J. Relefors, J. High Energy Phys. 05 (2014) 015.
[45] C. T. Sachrajda and G. Villadoro, Phys. Lett. B **609**, 73 (2005).
[46] C. Bernard, J. Bijnens, E. Gámiz, and J. Relefors, arXiv:1702.03416.
[47] J. Bijnens and P. Talavera, J. High Energy Phys. 03 (2002) 046.
[48] J. Noaki *et al.* (JLQCD and TWQCD Collaborations), Phys. Rev. Lett. **101**, 202004 (2008).
[49] J. Bijnens, G. Colangelo, and G. Ecker, J. High Energy Phys. 02 (1999) 020.
[50] The formulas for the loop corrections, $f_{+,4,L}$, $f_{+,4,B}$, $f_{-,4,L}$ and $f_{-,4,B}$, are available from the authors of Ref. [20] on request.
[51] J. Bijnens and G. Ecker, Annu. Rev. Nucl. Part. Sci. **64**, 149 (2014).
[52] J. Noaki *et al.* (JLQCD and TWQCD Collaborations), *Proc. Sci.*, LAT2009 (2010) 096, [arXiv:0910.5532].
[53] C. G. Callan and S. B. Treiman, Phys. Rev. Lett. **16**, 153 (1966).
[54] R. Dashen and M. Weinstein, Phys. Rev. Lett. **22**, 1337 (1969).
[55] V. Cirigliano, M. Knecht, H. Neufeld, H. Rupertsberger, and P. Talavera, Eur. Phys. J. C **23**, 121 (2002).
[56] A. Kastner and H. Neufeld, Eur. Phys. J. C **57**, 541 (2008).
[57] V. Cirigliano, M. Giannotti, and H. Neufeld, J. High Energy Phys. 11 (2008) 006.
[58] J. C. Hardy and I. S. Towner, *Proc. Sci.*, CKM2016 (2017) 028.
[59] C. Patrignani *et al.* (Particle Data Group Collaboration), Chin. Phys. C **40**, 100001 (2016).
[60] For a recent global analysis, see M. González-Alonso and J. M. Camalich, J. High Energy Phys. 12 (2016) 052.
[61] T. Kaneko *et al.* (JLQCD Collaboration), *Proc. Sci.*, LATTICE2013 (2014) 125, [arXiv:1311.6941].
[62] J. Noaki *et al.* (JLQCD Collaboration), *Proc. Sci.*, LATTICE2014 (2015) 069.
[63] B. Fahy, G. Cossu, and S. Hashimoto (JLQCD Collaboration), *Proc. Sci.*, LATTICE2016 (2017) 118, [arXiv:1702.02303].
[64] T. Kaneko, B. Fahy, H. Fukaya, and S. Hashimoto (JLQCD Collaboration), *Proc. Sci.*, LATTICE2016 (2017) 297, [arXiv:1701.00942].